

1 Pythia 8.3 tuning based on Belle fragmentation related
2 measurements

3 Ralf Seidl^{1,2,3}

4 ¹*Tokyo University, QNSI, Tokyo, Japan*

5 ²*RIKEN Nishina Center for Accelerator-Based Science, Wako, Saitama 351-0198, Japan*

6 ³*RIKEN-BNL Research Center, Upton New York 11973-5000, USA*

7 January 7, 2026
8 v. 1.0

9 **Abstract**

10 Belle has measured a large number of fragmentation-related results that
11 have been already successfully used in global fits of fragmentation functions.
12 These fragmentation functions are important input for studying the nucleon
13 structure in semi-inclusive Deeply inelastic lepton nucleon scattering and
14 hadron collisions. Apart from the additional flavor-sensitivity, also spin and
15 transverse momentum of partons in the nucleon can be accessed this way. Ad-
16 ditionally, these fragmentation-related results should be extremely sensitive
17 to the fragmentation parameters in Monte Carlo event generators. This note
18 concentrates on the tuning efforts of PYTHIA 8.3 using these measurements.

19 **Contents**

20 1 To-Do list and Changelog	8
21 1.1 README	8
22 1.2 To-Do list	8
23 2 Introduction	9
24 2.1 The Lund Model	9
25 3 Tuning Setup, prerequisites, etc	10
26 4 Data sets used in the fitting	10
27 4.1 BELLE_2017_I1606201	10
28 4.2 BELLE_2017_I1607562	10
29 4.3 BELLE_2019_I1718551	11
30 4.4 BELLE_2020_I1777678	11
31 4.5 BELLE_2024_I2849895	11
32 5 Sample generation, etc	11

³³	6	Individual sensitivities	15
³⁴	6.1	Single hadron cross sections	15
³⁵	6.2	Di-hadron cross sections	16
³⁶	6.3	Transverse momentum dependent cross sections	16
³⁷	7	Tuning fits	29
³⁸	7.1	Main hadrons	29
³⁹	7.2	Decaying and charmed mesons	29
⁴⁰	7.3	Di-hadrons in various configurations	33
⁴¹	7.4	Transverse momentum dependent cross sections	33
⁴²	7.5	Hyperons and charmed baryons	43
⁴³	8	Systematic uncertainties and tests	44
⁴⁴	8.1	Comparison to older settings	47
⁴⁵	9	Results	56
⁴⁶	A	Pythia StringZ:aExtraDiquark bugfix related changes	58

⁴⁷ List of Figures

⁴⁸	1	Correlation matrix of all parameters as obtained from a test tuning set that was run over 5000 parameters, a reduced set of data sets and only a third order interpolation in order to be computationally feasible at all.	13
⁴⁹	2	Correlation matrices of each tuning set separately, obtained from the last iterations of the nominal tuning procedure and interpolation based on 2000 parameter sets each, the full data sets and a 5th order polynomial interpolation.	14
⁵⁰	3	Sensitivities of the pion cross sections as a function of the fractional energy z . The different curves correspond to the sensitivities to the various tune parameters.	15
⁵¹	4	Sensitivities of the kaon cross sections as a function of the fractional energy z . The different curves correspond to the sensitivities to the various tune parameters.	16
⁵²	5	Sensitivities of the proton cross sections as a function of the fractional energy z . The different curves correspond to the sensitivities to the various tune parameters.	17
⁵³	6	Sensitivities of the ρ^0 cross sections as a function of the fractional energy x_p . The different curves correspond to the sensitivities to the various tune parameters.	18
⁵⁴	7	Sensitivities of the ω cross sections as a function of the fractional energy x_p . The different curves correspond to the sensitivities to the various tune parameters.	18

71	8	Sensitivities of the K^{*0} cross sections as a function of the fractional energy x_p . The different curves correspond to the sensitivities to the various tune parameters.	19
74	9	Sensitivities of the ϕ cross sections as a function of the fractional energy x_p . The different curves correspond to the sensitivities to the various tune parameters.	20
77	10	Sensitivities of the η cross sections as a function of the fractional energy x_p . The different curves correspond to the sensitivities to the various tune parameters.	20
80	11	Sensitivities of the D^+ cross sections as a function of the fractional energy x_p . The different curves correspond to the sensitivities to the various tune parameters.	21
83	12	Sensitivities of the D^{*0} cross sections as a function of the fractional energy x_p . The different curves correspond to the sensitivities to the various tune parameters.	22
86	13	Sensitivities of the $\pi^+\pi^-$ cross sections as a function of the invariant mass, in the z bin . The different curves correspond to the sensitivities to the various tune parameters.	23
89	14	Sensitivities of the π^+K^- cross sections as a function of the invariant mass, in the z bin . The different curves correspond to the sensitivities to the various tune parameters.	24
92	15	Sensitivities of the K^+K^- cross sections as a function of the invariant mass, in the z bin. The different curves correspond to the sensitivities to the various tune parameters.	25
95	16	Sensitivities of the π cross sections as a function of the transverse momentum in the z bin and a thrust value of $0.8 - 0.9$. The different curves correspond to the sensitivities to the various tune parameters.	26
98	17	Sensitivities of the π cross sections as a function of the transverse momentum in the z bin and a thrust value of $0.8 - 0.9$. The different curves correspond to the sensitivities to the various tune parameters.	27
101	18	Sensitivities of the π cross sections as a function of the transverse momentum in the z bin and a thrust value of $0.8 - 0.9$. The different curves correspond to the sensitivities to the various tune parameters.	28
104	19	Pion cross sections as a function of the fractional energy z . The data is displayed by black points while the best fit result in red.	29
106	20	Kaon cross sections as a function of the fractional energy z . The data is displayed by black points while the best fit result in red.	30
108	21	Proton cross sections as a function of the fractional energy z . The data is displayed by black points while the best fit result in red.	31
110	22	Left: neutral ρ cross sections as a function of the fractional momentum x_p . Right: charged ρ cross sections. The data is displayed by black points while the best fit result in red.	31
113	23	Left: neutral K^* cross sections as a function of the fractional momentum x_p . Right: charged K^* cross sections. The data is displayed by black points while the best fit result in red.	32

116	24	Left: ω cross sections as a function of the fractional momentum x_p . Right: ϕ cross sections. The data is displayed by black points while the best fit result in red. The missing χ^2 is 3.96.	32
117			
118	25	Left: η cross sections as a function of the fractional momentum x_p . Right: K_S cross sections. The data is displayed by black points while the best fit result in red.	33
119			
120	26	Left: D^+ cross sections as a function of the fractional momentum x_p . Right: D^0 cross sections. The data is displayed by black points while the best fit result in red.	34
121			
122	27	Left: D^{*+} cross sections as a function of the fractional momentum x_p . Right: D^{*0} cross sections. The data is displayed by black points while the best fit result in red.	34
123			
124	28	Left: D_s^+ cross sections as a function of the fractional momentum x_p . Right: D_s^{*+} cross sections. The data is displayed by black points while the best fit result in red.	35
125			
126	29	Left: $\pi^+\pi^-$ pair cross sections as a function of the invariant mass m for the fractional energy bin $0.3 - 0.35$. Right: The same for the fractional energy bin $0.7 - 0.75$. The data is displayed by black points while the best fit result in red.	35
127			
128	30	Left: $\pi^+\pi^+$ pair cross sections as a function of the invariant mass m for the fractional energy bin $0.3 - 0.35$. Right: The same for the fractional energy bin $0.7 - 0.75$. The data is displayed by black points while the best fit result in red.	36
129			
130	31	Left: π^+K^- pair cross sections as a function of the invariant mass m for the fractional energy bin $0.3 - 0.35$. Right: The same for the fractional energy bin $0.6 - 0.65$. The data is displayed by black points while the best fit result in red.	36
131			
132	32	Left: π^+K^+ pair cross sections as a function of the invariant mass m for the fractional energy bin $0.3 - 0.35$. Right: The same for the fractional energy bin $0.7 - 0.75$. The data is displayed by black points while the best fit result in red.	37
133			
134	33	Left: K^+K^- pair cross sections as a function of the invariant mass m for the fractional energy bin $0.3 - 0.35$. Right: The same for the fractional energy bin $0.7 - 0.75$. The data is displayed by black points while the best fit result in red.	37
135			
136	34	Left: K^+K^+ pair cross sections as a function of the invariant mass m for the fractional energy bin $0.35 - 0.4$. Right: The same for the fractional energy bin $0.7 - 0.75$. The data is displayed by black points while the best fit result in red.	38
137			
138	35	Left: $\pi^+\pi^-$ pair cross sections in opposite hemispheres as a function of the invariant mass z_2 for the fractional energy bin $0.25 < z_1 < 0.3$. Right: The same for the fractional energy bin $0.55 < z_1 < 0.6$. The data is displayed by black points while the best fit result in red.	38
139			
140			
141			
142			
143			
144			
145			
146			
147			
148			
149			
150			
151			
152			
153			
154			
155			
156			
157			
158			

203	48	Strange quark related vector meson and higher spin variables as a function of the various tuning iterations, the allowed ranges are shown in shaded regions and the best values as the center line. Dashed lines represent variables that have been fixed after they became stable.	45
204			
205			
206			
207	49	Charm quark related vector meson and higher spin variables as a function of the various tuning iterations, the allowed ranges are shown in shaded regions and the best values as the center line. Dashed lines represent variables that have been fixed after they became stable.	46
208			
209			
210			
211	50	Baryon related variables as a function of the various tuning iterations, the allowed ranges are shown in shaded regions and the best values as the center line. Dashed lines represent variables that have been fixed after they became stable.	46
212			
213			
214			
215	51	Mixing related variables as a function of the various tuning iterations, the allowed ranges are shown in shaded regions and the best values as the center line. Dashed lines represent variables that have been fixed after they became stable.	47
216			
217			
218			
219	52	Evolution of the goodness of fit normalized by the number of degrees of freedom as a function of the various tuning iterations.	47
220			
221	53	Pion cross sections as a function of the fractional energy z . The data is displayed by black points while the PYTHIA default is displayed in red, the current Belle2 setting in blue, and the best tune in green.	48
222			
223			
224	54	Kaon cross sections as a function of the fractional energy z . The data is displayed by black points while the PYTHIA default is displayed in red, the current Belle2 setting in blue, and the best tune in green.	49
225			
226			
227	55	Proton cross sections as a function of the fractional energy z . The data is displayed by black points while the PYTHIA default is displayed in red, the current Belle2 setting in blue, and the best tune in green.	50
228			
229			
230	56	Top: $\pi^+\pi^-$ spectra as a function of z_2 for two bins of z_1 . Bottom: $\pi^\pm\pi^\pm$ spectra for the same z bins. The data is displayed by black points while the PYTHIA default is displayed in red, the current Belle2 setting in blue, and the best tune in green.	51
231			
232			
233			
234	57	Top: π^+K^- spectra as a function of z_2 for two bins of z_1 . Bottom: $\pi^\pm K^\pm$ spectra for the same z bins. The data is displayed by black points while the PYTHIA default is displayed in red, the current Belle2 setting in blue, and the best tune in green.	52
235			
236			
237			
238	58	Top: K^+K^- spectra as a function of z_2 for two bins of z_1 . Bottom: $K^\pm K^\pm$ spectra for the same z bins. The data is displayed by black points while the PYTHIA default is displayed in red, the current Belle2 setting in blue, and the best tune in green.	53
239			
240			
241			
242	59	Left: A spectrum as a function of x_p . Right Σ^0 spectrum as a function of x_p . The data is displayed by black points while the PYTHIA default is displayed in red, the current Belle2 setting in blue, and the best tune in green.	54
243			
244			
245			

246	60	Left: Λ_c^+ spectrum as a function of x_p . Right $\Sigma_c^0(2455)$ spectrum as a function of x_p . The data is displayed by black points while the PYTHIA default is displayed in red, the current Belle2 setting in blue, and the best tune in green.	54
247	61	Comparison of the distributions for protons (top left), Λ (top right), Σ^0 (bottom left) and Σ^{*+} as a function of energy or momentum fraction. The black points correspond to the measurements while the yellow points correspond to the best values after tune 71 using PYTHIA8.3.13, the green points correspond to the same tune but using PYTHIA8.3.16, the blue points use the same but explicitly setting StringZ:useOldAExtra to "on", and the red points correspond to the same, but switching it to "off".	59
248	62	Comparison of the distributions for Ξ^- (top left), Λ_c (top right), $\Sigma_c^0(2455)$ (bottom left) and $\Sigma_c^0(2520)$ as a function of momentum fraction. The black points correspond to the measurements while the yellow points correspond to the best values after tune 71 using PYTHIA8.3.13, the green points correspond to the same tune but using PYTHIA8.3.16, the blue points use the same but explicitly setting StringZ:useOldAExtra to "on", and the red points correspond to the same, but switching it to "off".	60
249			
250			
251			
252			
253			
254			
255			
256			
257			
258			
259			
260			
261			
262			
263			
264			
265			

²⁶⁶ **1 To-Do list and Changelog**

²⁶⁷ **1.1 README**

²⁶⁸ **1.2 To-Do list**

²⁶⁹ • add sensitivity discussion for popcorn variables

270 2 Introduction

271 Fragmentation describes the formation of confined final-state hadrons from high-
272 energetic, asymptotically free partons. Just as parton distribution functions, they
273 cannot be calculated from first principles in QCD and therefore need to be extracted
274 experimentally. For the same reason, also Monte Carlo event generators have to use
275 models to describe this. One of the most commonly used models is the Lund string
276 fragmentation model. While the Lund model can describe the fragmentation reason-
277 ably well, overall, it relies on many parameters that need to be tuned using data.
278 In this note this tuning was performed systematically on the various fragmentation
279 measurements that contain sensitivities to the main Lund parameters, the suppres-
280 sion of strange quark pairs produced in the fragmentation, the suppression of η
281 mesons, the suppression of di-quark pair production needed to create baryons in the
282 fragmentation, the transverse momentum generated in the fragmentation, and the
283 role vector mesons and higher spin particle production has over the pseudoscalar
284 production, etc.

285 In the following the procedure to tune the fragmentation parameters are dis-
286 cussed. Initially the different types of software and their setups are discussed. Then,
287 the sensitivities of the used measurements to the relevant variables are discussed
288 before the actual fit results and best tune parameters are presented and discussed.

289 2.1 The Lund Model

290 The Lund String fragmentation model [1, 2] is the main model that tries to describe
291 the fragmentation process. It generally describes e^+e^- fragmentation into hadrons as
292 the separation of singlet (anti)quarks moving away from each other within a linear
293 potential that quasi-classically describes the QCD confining potential. The linear
294 potential can be thought of being caused by a string of gluons connecting the two
295 color charges. This string then eventually breaks up into a quark-antiquark pair
296 (or also diquark-antidiquark pair). These resulting (anti-)quarks either coalesce into
297 hadrons or expand further, creating even more quark-antiquark pairs in the process.
298 In this stochastic process particles are then produced according to

$$f(z) = N \frac{1}{z} (1-z)^a \exp\left(-\frac{bm^2}{z}\right) \quad (1)$$

299 where a defines how fast the function vanishes at high- z and b is related to the mass
300 created at a certain z , and z is the energy fraction a hadron carries relative to the
301 initial parton energy. Furthermore, this generation does not have to necessarily fol-
302 low on the lightcone, but can also happen at transverse coordinates, thus allowing
303 for transverse momentum to be generated relative to the initially separating par-
304 tons. Empirically, not all quark-antiquark pairs can be created equally, as heavier
305 quarks are less likely to be created in the fragmentation process. For this purpose
306 a parameter was introduced that describes the suppression of strangeness relative
307 to light quark flavors. The model is initially also not a priori able to distinguish
308 between what spin-state a certain hadron that was created has. Therefore parame-
309 ters for vector meson generation over pseudo-scalar generation for light, strange and

310 charm quarks are introduced, as well as similar parameters for spin, orbital angular
311 and total angular momenta up to 2 are introduced.

312 **3 Tuning Setup, prerequisites, etc**

313 For the general setup, Pythia 8.3.12 (later also 8.3.16 to be discussed below, see A)
314 was used where the main144 code of the examples section was utilized to enable
315 the facility to parse input files and provide yoda output files that are using the
316 RIVET analysis codes for the data sets specified below. RIVET4.0.1 was used for
317 the analysis codes, Rivet plotting and the actual data yoda files. A few significant
318 exceptions to this are that the most recent Belle measurements for light and charmed
319 mesons [3] were not available yet, therefore yoda data files, Rivet analysis codes
320 and plotting instructions were created personally to include them in the tuning.
321 Similarly, a few issues were found in the official RIVET codes that were fixed locally.
322 Those include a switching of the ordering of integrated hyperon and charmed baryon
323 cross sections relative to those differential in the momentum fraction. Also for the
324 transverse momentum dependent measurements, the fractional energy z binning in
325 the codes was off by one bin for protons that would be physically impossible to
326 cover at Belle energies due to its mass. Also for some measurements the treatment
327 of weak decays was inaccurate as only charmed decays were removed in the RIVET
328 codes while other weak decays were kept, in contrast to the actual measurements.
329 Therefore the weak-decay removed measurements that include pions or protons were
330 not included in the fitting procedure. The tune optimization was performed using
331 the Professor2.5 package [4].

332 **4 Data sets used in the fitting**

333 For the fitting, the following measurements were used, ordered by publication time:

334 **4.1 BELLE_2017_I1606201**

335 These measurements include various hyperon and charmed baryon final states as
336 a function of the fractional momentum x_p and the total production cross sections
337 [5]. Because of these, these measurements are particularly sensitive to the Baryon
338 production related PYTHIA variables.

339 **4.2 BELLE_2017_I1607562**

340 These measurements contain the invariant mass and fractional energy dependent
341 cross sections for same and opposite charged pairs of pions and kaons within the
342 same hemisphere [6]. As such, they provide information on the various mass peaks
343 in their range and therefore also indirectly on higher spin and orbital momentum
344 particles that feed into these spectra.

³⁴⁵ 4.3 BELLE_2019_I1718551

³⁴⁶ These measurements contain the cross sections of pions, kaons and protons as a
³⁴⁷ function of energy fraction z and transverse momentum relative to the thrust axis,
³⁴⁸ in bins of the thrust value [7]. Therefore they are most sensitive to the transverse
³⁴⁹ momentum generation in the fragmentation, but indirectly also the main LUND
³⁵⁰ related fragmentation variables, etc.

³⁵¹ 4.4 BELLE_2020_I1777678

³⁵² In this publication the cross sections as a function of fractional energy z for pions,
³⁵³ kaons and protons are included, being likely sensitive to the main Lund fragmenta-
³⁵⁴ tion parameters, as well as the baryon related ones for the protons [8]. Additionally,
³⁵⁵ also pairs of pions or kaons in same or opposite hemispheres as well as any pairs are
³⁵⁶ measured as function of the fractional energies of each hadron. Apart from the nom-
³⁵⁷ inal fractional energy definition two alternate definitions are also included, however
³⁵⁸ for this exercise they were not included in the tuning effort since those would be
³⁵⁹ mostly redundant.

³⁶⁰ 4.5 BELLE_2024_I2849895

³⁶¹ This is the newest result, just published earlier in 2025, and contains a larger number
³⁶² of cross sections differential in the momentum fraction x_p for various lighter and
³⁶³ charmed mesons decaying into two or three pions or kaons, many for the first time
³⁶⁴ at B factories [3]. This data set is most sensitive to the pseudo-scalar to vector-
³⁶⁵ meson ratios, the η suppression, the light pseudo-scalar and vector mixing angles,
³⁶⁶ and indirectly also the higher spin resonances.

³⁶⁷ 5 Sample generation, etc

³⁶⁸ Given that the number of datasets that are used are very large, it was not possible
³⁶⁹ to fit all tuning parameters at the same time. Instead, parameter sets of 6 to 8
³⁷⁰ were optimized simultaneously while iterating over all relevant parameters and pre-
³⁷¹ forming the optimization many times to avoid running into local minima. In each
³⁷² iteration the best values of the previous tune were set while the next set of variables
³⁷³ were allowed to float. In the initial iterations the parameter ranges were mostly
³⁷⁴ identical to the allowed ranges in PYTHIA while in the later iterations, the ranges
³⁷⁵ were narrowed down somewhat for variables that were very stable over the previous
³⁷⁶ steps. In PROFESSOR, the initial configurations are randomly created based on the
³⁷⁷ boundaries of the variables to optimize using the command *prof2-sample*. In earlier
³⁷⁸ iterations about 500 to 1000 samples were generated while in the later stages 2000
³⁷⁹ samples were generated. This ensured that the interpolation of the parameter tunes
³⁸⁰ and responses could be performed using 5th order polynomials, still. For each sample
³⁸¹ initially 1.2 M and later 5 M $e^+e^- \rightarrow q\bar{q}$ events were generated for uds and charm
³⁸² flavors together. As all these measurements had already been corrected for non- $q\bar{q}$

Table 1: Parameters used in the tuning, their PYTHIA8.3 default values, the BelleII default values (as of release-09-00-01 in generators/modules/fragmentation/-data/pythia_belle2.charm.dat), empty if PYTHIA 8.2 default value is used, the best value after the tuning and a brief explanation of the parameter.

Variable	P8.3	Belle2	Best	description
StringZ:aLund	0.68	0.32	0.525	(1-z) power
StringZ:bLund	0.98	0.62	0.910	Transverse mass term
StringPT:sigma	0.335		0.372	Transverse momentum in fragmentation
StringFlav:probStoUD	0.217	0.286	0.240	Strangeness suppression wrt to ud quarks
StringFlav:etaSup	0.60		0.850	Extra eta suppression
StringFragmentation:stopMass	1.0	0.3	0.831	Stop mass (End point condition?)
StringFlav:mesonUDVector	0.50		0.554	Vector to PS ratio light quarks
StringFlav:mesonUDL1S0J1	0.0		0.311	Higher spin states L=1, S=0, J=1 light q
StringFlav:mesonUDL1S1J0	0.0		0.236	Higher spin states L=1, S=1, J=0 light q
StringFlav:mesonUDL1S1J1	0.0		0.267	Higher spin states L=1, S=1, J=1 light quarks
StringFlav:mesonUDL1S1J2	0.0		0.400	Higher spin states L=1, S=1, J=2 light quarks
StringFlav:mesonSvector	0.55		0.870	Vector to PS ratio strange quarks
StringFlav:mesonSDL1S0J1	0.0		0.118	Higher spin states L=1, S=0, J=1 s quarks
StringFlav:mesonSDL1S1J0	0.0		0.374	Higher spin states L=1, S=1, J=0 s quarks
StringFlav:mesonSDL1S1J1	0.0		0.365	Higher spin states L=1, S=1, J=1/2 s quarks
StringFlav:mesonSDL1S1J2	0.0		0.588	Higher spin states L=1, S=1, J=1/2 s quarks
StringZ:rFactC	1.32	1.0	0.410	Bowler modification for charm quarks
StringFlav:mesonCvector	0.88	2.8	2.226	Vector to PS ratio charm quarks
StringFlav:mesonCDL1S0J1	0.0	0.06	1.729	Higher spin states L=1, S=0, J=1 charm
StringFlav:mesonCDL1S1J0	0.0	0.1775	0.635	Higher spin states L=1, S=1, J=0 charm
StringFlav:mesonCDL1S1J1	0.0	0.1868	2.644	Higher spin states L=1, S=1, J=1 charm
StringFlav:mesonCDL1S1J2	0.0	0.1836	1.972	Higher spin states L=1, S=1, J=2 charm
StringFlav:thetaPS	-15		-15.71	Mixing angle for PS mesons
StringFlav:thetaV	36		27.08	Mixing angle for V mesons
StringFlav:probQQtoQ	0.081	0.133	0.064	Diquark over quark ratio
StringZ:aExtraDiquark	0.97		1.696	Lund extra a term for diquarks(baryons)
StringFlav:probSQtoQQ	0.9156	0.323	0.521	Strange over light diquark suppression
StringFlav:probQQ1toQQ0	0.0275	0.0468	0.252	Vector over scalar diquark suppression
StringFlav:popcornRate			0.055112	mesons between diquark pairs
StringFlav:popcornSpair			0.106073	strange Popcorn diquark
StringFlav:popcornSmeson			0.447140	strange meson in Popcorn

383 contributions, no other hard processes are included. Also ISR had been corrected in
 384 the measurements so it was switched off in the MC generation as well.

385 The following sets of parameters were optimized together initially:

- 386 • Set A (main Lund): StringZ:aLund, StringZ:bLund, StringPT:sigma, StringFlav:probStoUD,
 387 StringFlav:etaSup, StringFragmentation:stopMass
- 388 • Set B (baryons and charm): StringFlav:probQQtoQ, StringFlav:probSQtoQQ,
 389 StringFlav:probQQ1toQQ0, StringZ:aExtraDiquark, StringZ:rFactC, StringFlav:mesonCvector
 390 StringFlav:mesonCL1S0J1, StringFlav:mesonCL1S1J0
- 391 • Set C (vector mesons, mixing): StringFlav:mesonUDvector, StringFlav:mesonUDL1S0J1,
 392 StringFlav:mesonUDL1S1J0, StringFlav:mesonSvector, StringFlav:mesonSL1S0J1,
 393 StringFlav:mesonSL1S1J0, StringFlav:thetaPS, StringFlav:thetaV
- 394 • Set D (higher spin states): StringFlav:mesonUDL1S1J1, StringFlav:mesonUDL1S1J2,
 395 StringFlav:mesonSL1S1J1, StringFlav:mesonSL1S1J2, StringFlav:mesonCL1S1J1,

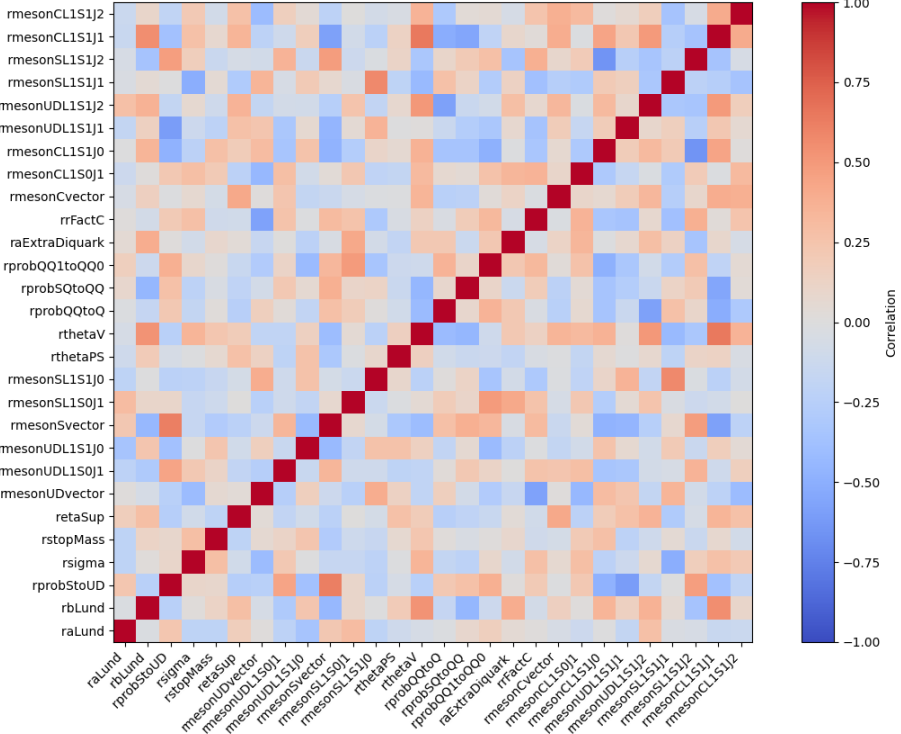


Figure 1: Correlation matrix of all parameters as obtained from a test tuning set that was run over 5000 parameters, a reduced set of data sets and only a third order interpolation in order to be computationally feasible at all.

396 **StringFlav:mesonCL1S1J2**

397 As can be seen in Fig. 1, all these 28 parameters are not uncorrelated, nor do the
 398 parameters of each set factorize either but generally they are somewhat less corre-
 399 lated between sets. Because of this an iterative approach was used where sets A to D
 400 were optimized several times after optimizing each set first (i.e. A → B → C → D → A → B → etc.)
 401 The individual correlation matrices after the last iteration of each tuning set are
 402 shown in Fig. 2. As one can see, within a tuning set correlations are more pro-
 403 nounced, most notably between the main two Lund parameters, but also, to a lesser
 404 extend between others.

405 At later iterations of the optimization, the more stable variables were retired
 406 (StringPT:sigma, StringFlav:probStoUD, StringFlav:mesonUDvector, StringFlav:probQQtoQ),
 407 using their best values from then on, but including the additional higher spin states
 408 and eventually the popcorn variables. The later settings therefore became:

- 409 • Set A' (main Lund): StringZ:aLund, StringZ:bLund, StringFlav:etaSup, StringFrag-
 410 mentation:stopMass, mesonUDL1S0J1, mesonUDL1S1J0
- 411 • Set B' (baryons): StringFlav:probSQtoQQ, StringFlav:probQQ1toQQ0, StringZ:aExtraDiquark
 412 popcornRate, StringFlav:popcornSpair, StringFlav:popcornSmeson
- 413 • Set C' (strange+mixing): StringFlav:mesonSvector, StringFlav:mesonSL1S0J1,

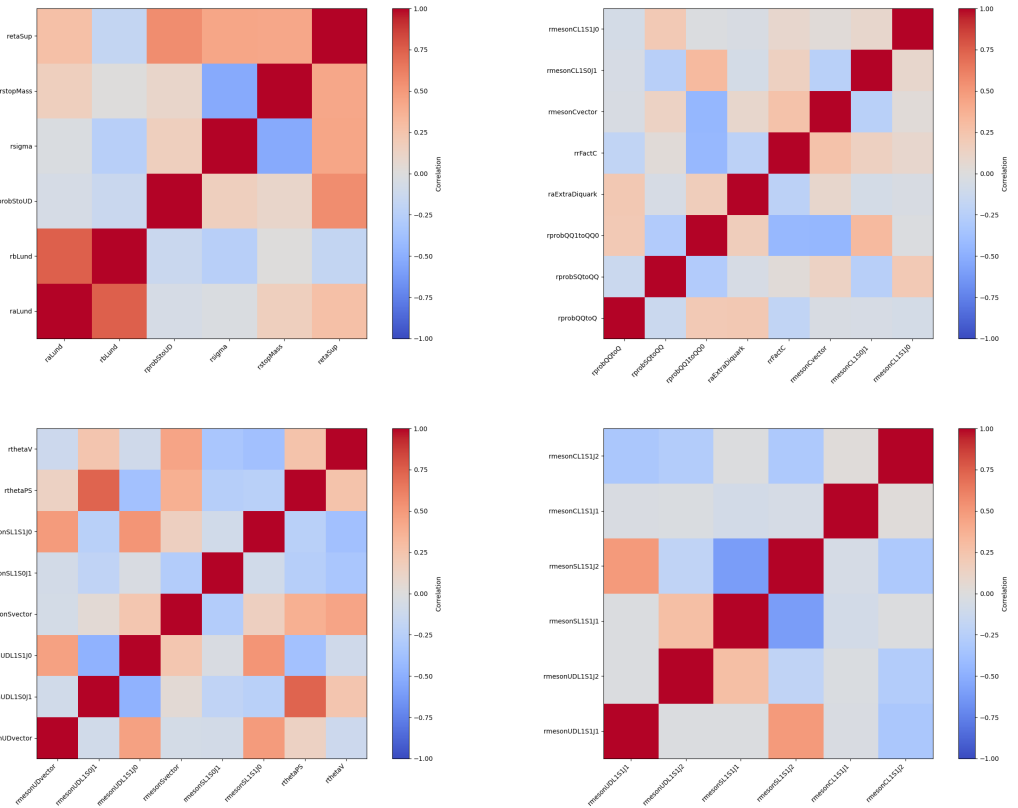


Figure 2: Correlation matrices of each tuning set separately, obtained from the last iterations of the nominal tuning procedure and interpolation based on 2000 parameter sets each, the full data sets and a 5th order polynomial interpolation.

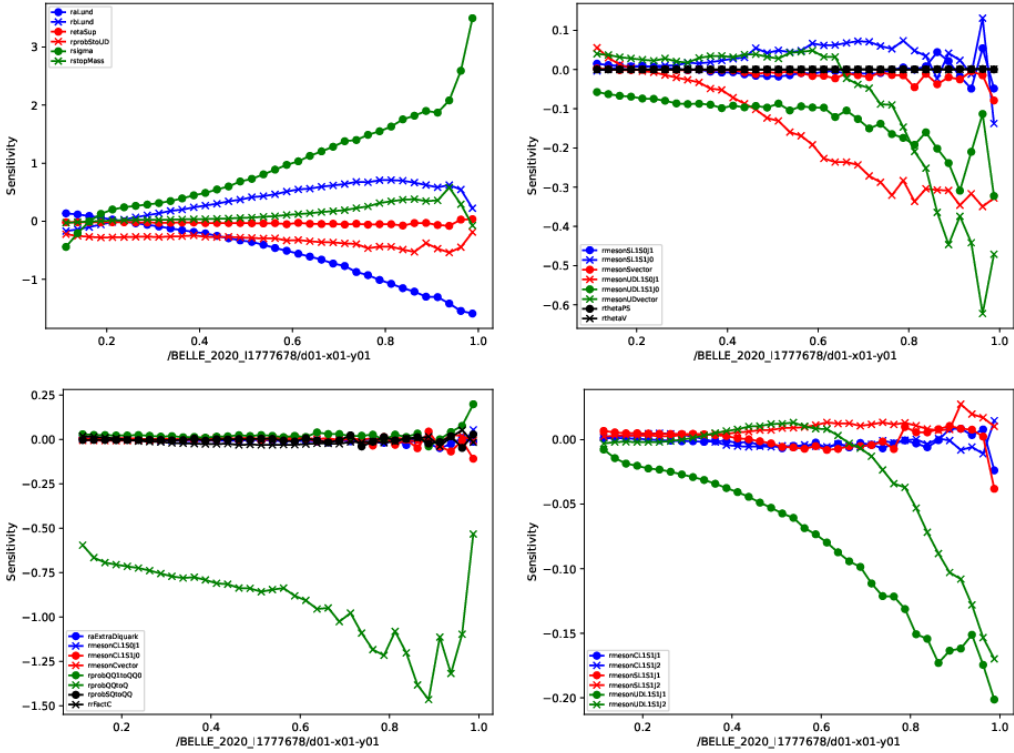


Figure 3: Sensitivities of the pion cross sections as a function of the fractional energy z . The different curves correspond to the sensitivities to the various tune parameters.

414 StringFlav:mesonSL1S1J0, StringFlav:mesonSL1S1J1, StringFlav:mesonSL1S1J2,
 415 StringFlav:thetaPS, StringFlav:thetaV

416 • Set D' (charm): StringZ:rFactC, StringFlav:mesonCvector, StringFlav:mesonCL1S0J1,
 417 StringFlav:mesonCL1S1J0, StringFlav:mesonCL1S1J1, StringFlav:mesonCL1S1J2

418 6 Individual sensitivities

419 In the following the individual sensitivities to the various tune parameters are shown
 420 for several of the key measurements.

421 6.1 Single hadron cross sections

422 This single pion cross sections have naturally a very high sensitivity to the main Lund
 423 fragmentation parameters, as well as to the fragmentation transverse momentum as
 424 can be seen in Fig. 3. There is also some sensitivity to the light quark vector mesons
 425 to pseudoscalar ratios and higher spin states. For kaons the sensitivities are similar
 426 except that strangeness suppression and the corresponding strange quark VM and
 427 higher spin variables are more sensitive as can be seen in Fig. 4. Protons in contrast
 428 are mostly sensitive to the diquark ratio and to a lesser extend the main lund
 429 parameters.

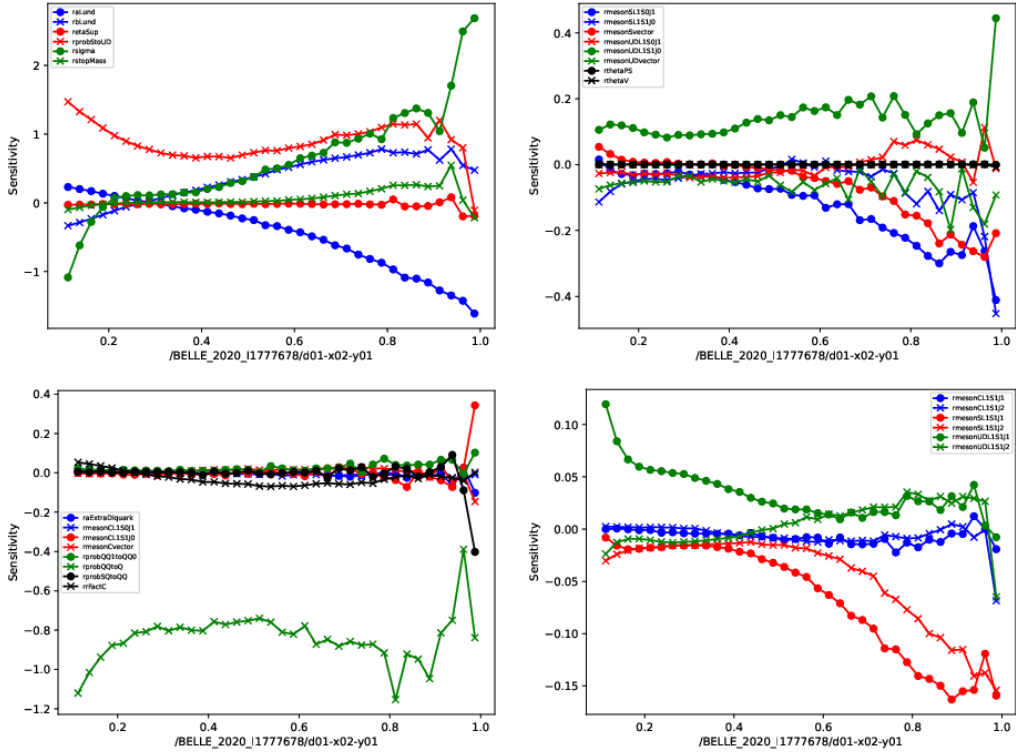


Figure 4: Sensitivities of the kaon cross sections as a function of the fractional energy z . The different curves correspond to the sensitivities to the various tune parameters.

430 For the vector mesons cross sections, the vector mesons variables for the relevant
 431 flavors are clearly the most sensitive parameters as can be seen in Fig. 6 for the ρ
 432 mesons, Fig. 7 for the ω Fig. 8, for the K^* and Fig. 9 for the ϕ mesons. The strange
 433 mesons do also have some sensitivity to the strangeness suppression again.

434 The η mesons naturally are most sensitive to the eta suppression parameter while
 435 they also provide a small sensitivity to the pseudoscalar mixing angle, apart from
 436 the regular Lund parameters, as shown in Fig. 10.

437 The charmed mesons obtain additional sensitivity to the extra charm term for
 438 the fragmentation, as well as for the vector mesons to the charmed VM hand higher
 439 spin state variables.

440 6.2 Di-hadron cross sections

441 For the di-hadron cross sections, again the vector mesons components appear in
 442 the vicinity of their masses, while additionally some sensitivity to the higher spin
 443 mesons is visible, particularly at higher masses as those can mostly be only indirectly
 444 obtained in these di-hadron spectra.

445 6.3 Transverse momentum dependent cross sections

446 The transverse momentum dependent cross sections naturally have a very high sen-
 447 sitivity to the transverse momentum generated in the fragmentation process as can

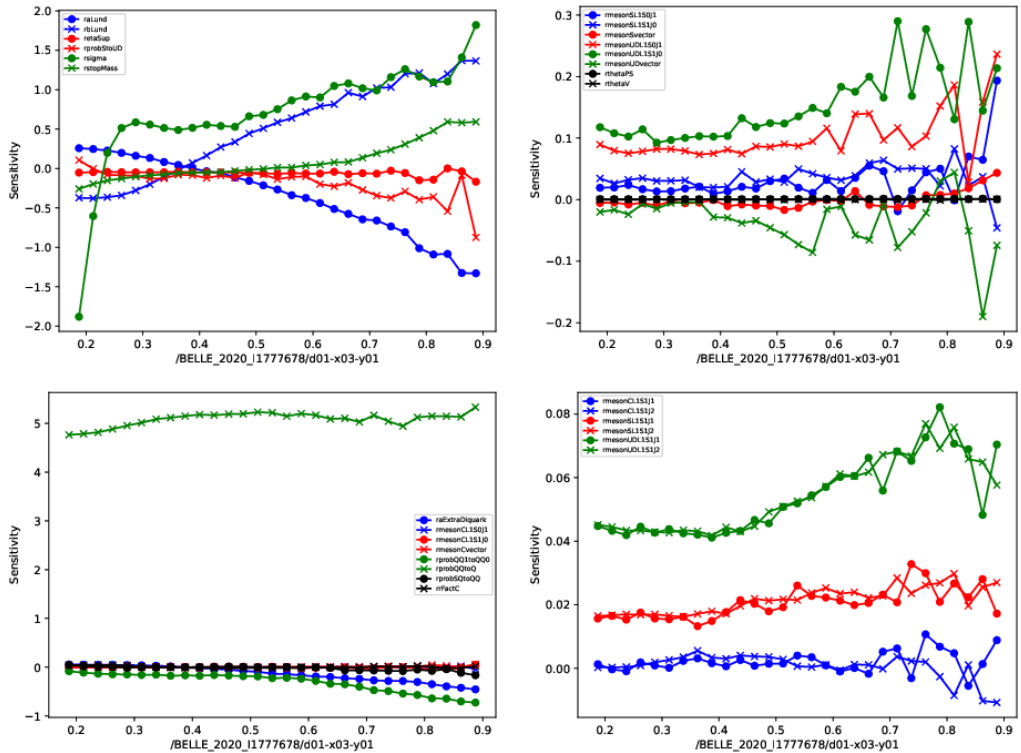


Figure 5: Sensitivities of the proton cross sections as a function of the fractional energy z . The different curves correspond to the sensitivities to the various tune parameters.

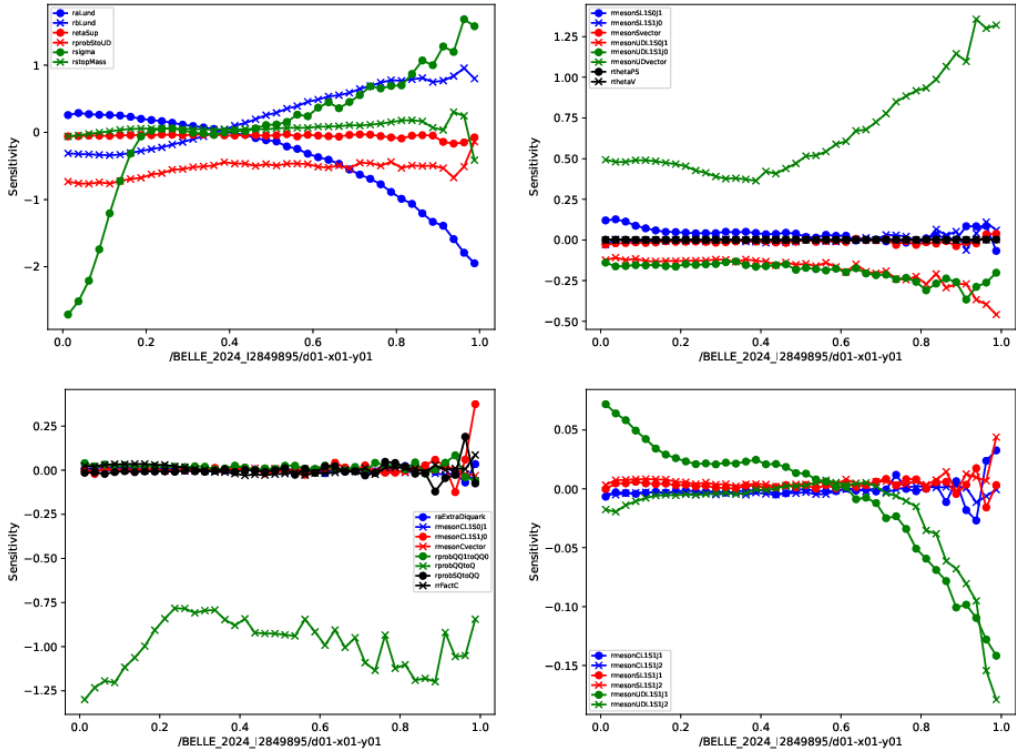


Figure 6: Sensitivities of the ρ^0 cross sections as a function of the fractional energy x_p . The different curves correspond to the sensitivities to the various tune parameters.

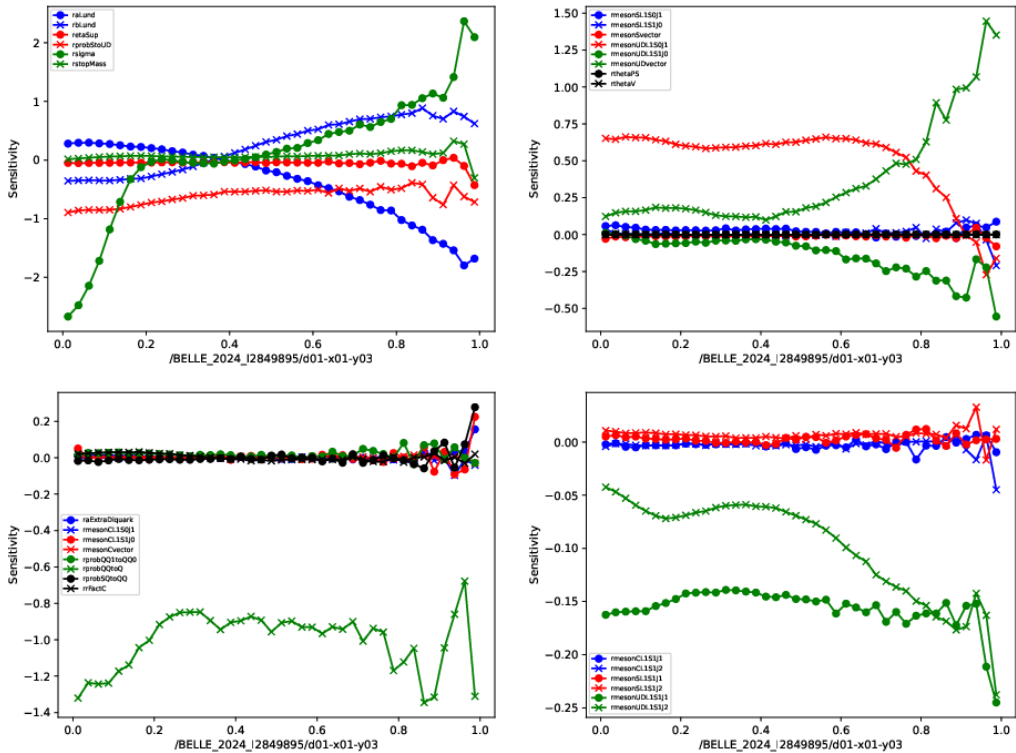


Figure 7: Sensitivities of the ω cross sections as a function of the fractional energy x_p . The different curves correspond to the sensitivities to the various tune parameters.

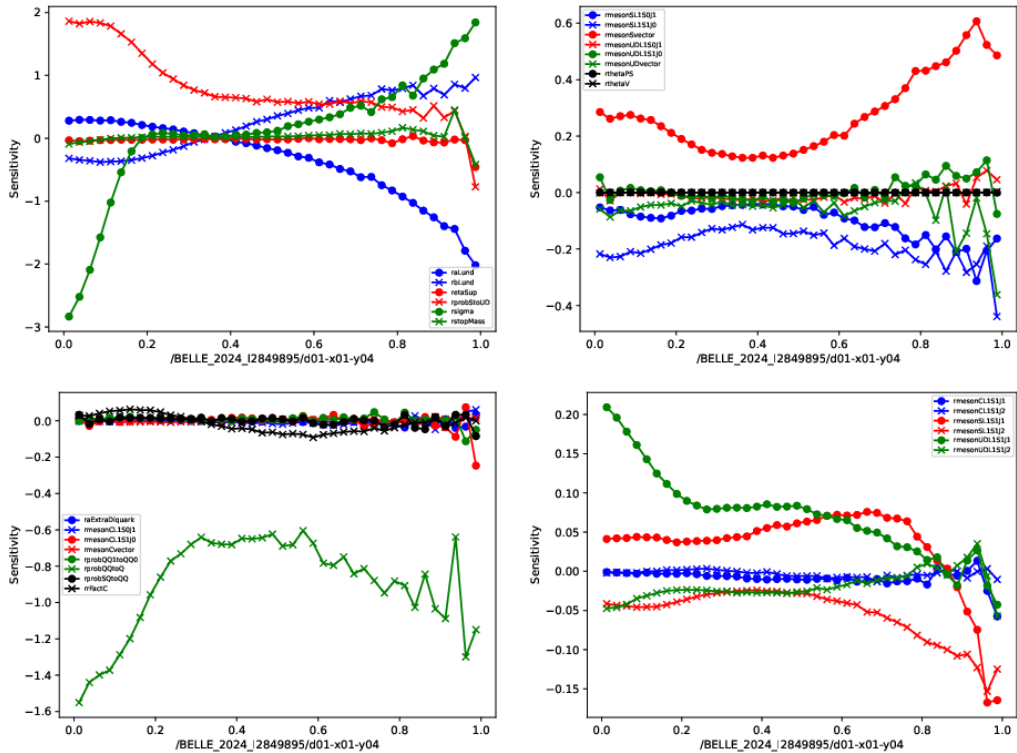


Figure 8: Sensitivities of the K^{*0} cross sections as a function of the fractional energy x_p . The different curves correspond to the sensitivities to the various tune parameters.

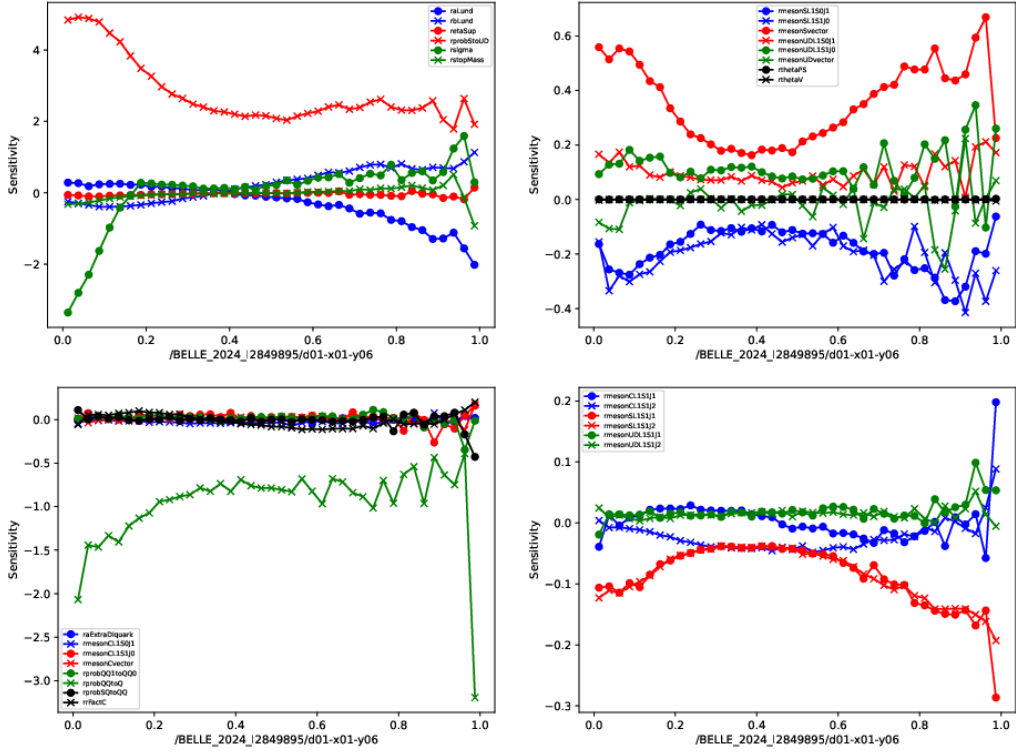


Figure 9: Sensitivities of the ϕ cross sections as a function of the fractional energy x_p . The different curves correspond to the sensitivities to the various tune parameters.

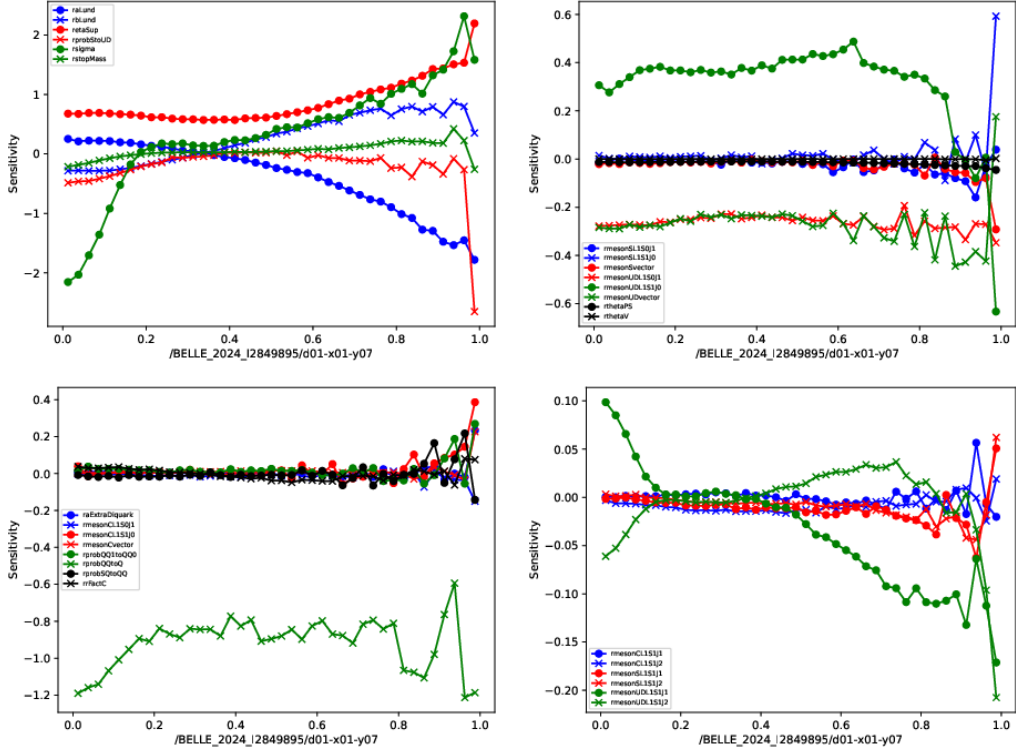


Figure 10: Sensitivities of the η cross sections as a function of the fractional energy x_p . The different curves correspond to the sensitivities to the various tune parameters.

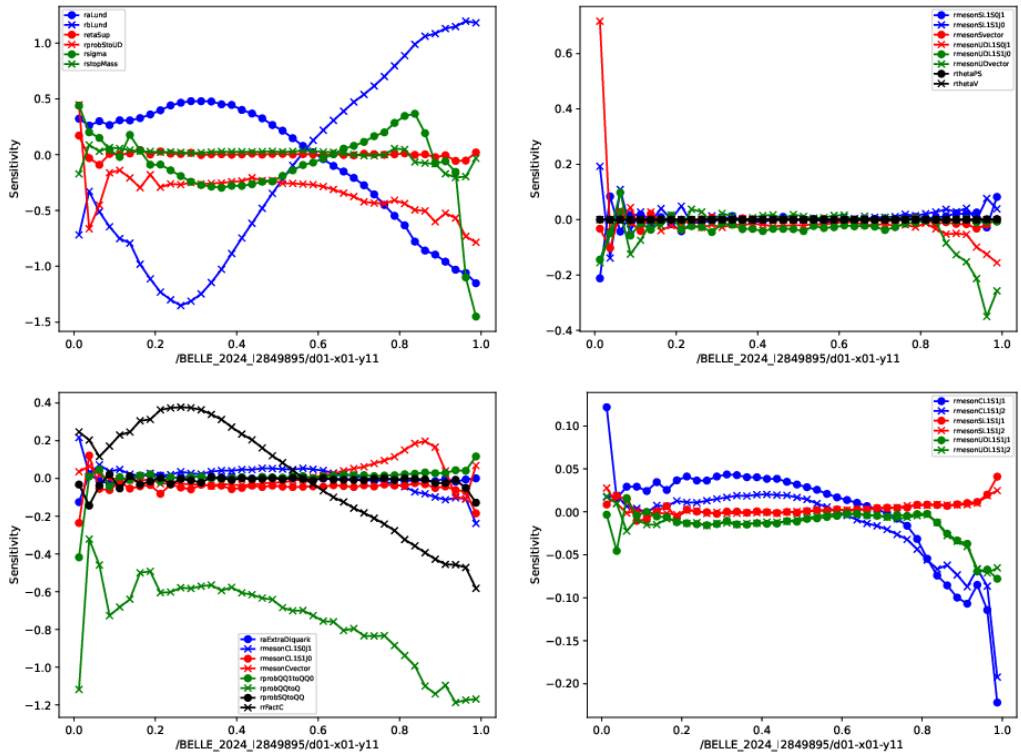


Figure 11: Sensitivities of the D^+ cross sections as a function of the fractional energy x_p . The different curves correspond to the sensitivities to the various tune parameters.

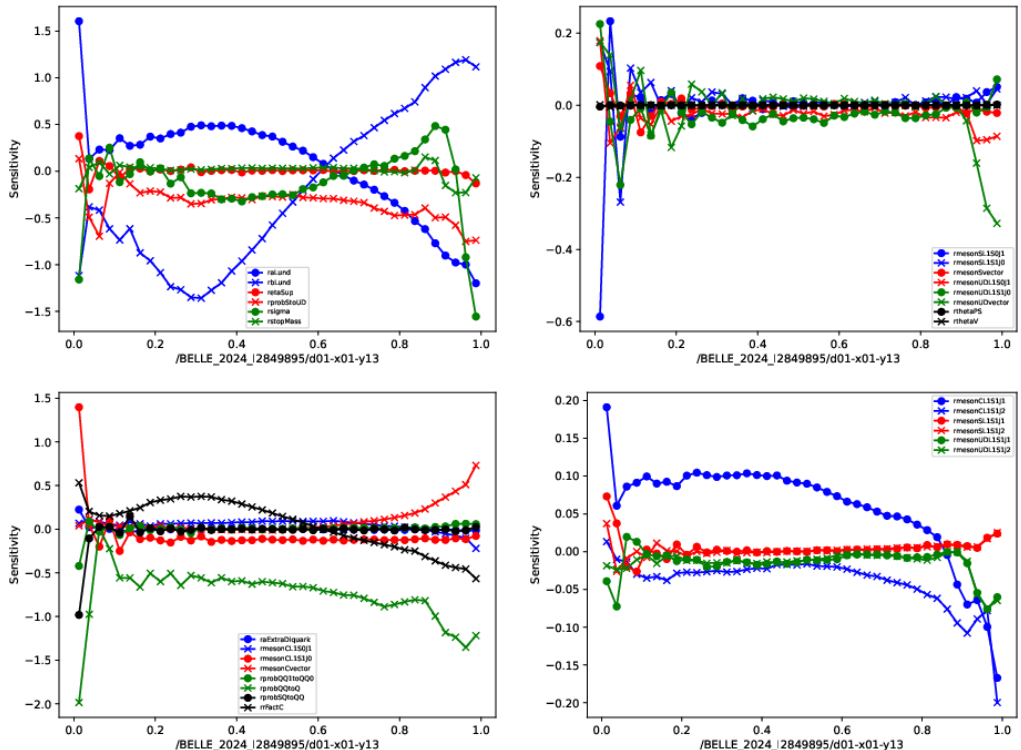


Figure 12: Sensitivities of the D^{*0} cross sections as a function of the fractional energy x_p . The different curves correspond to the sensitivities to the various tune parameters.

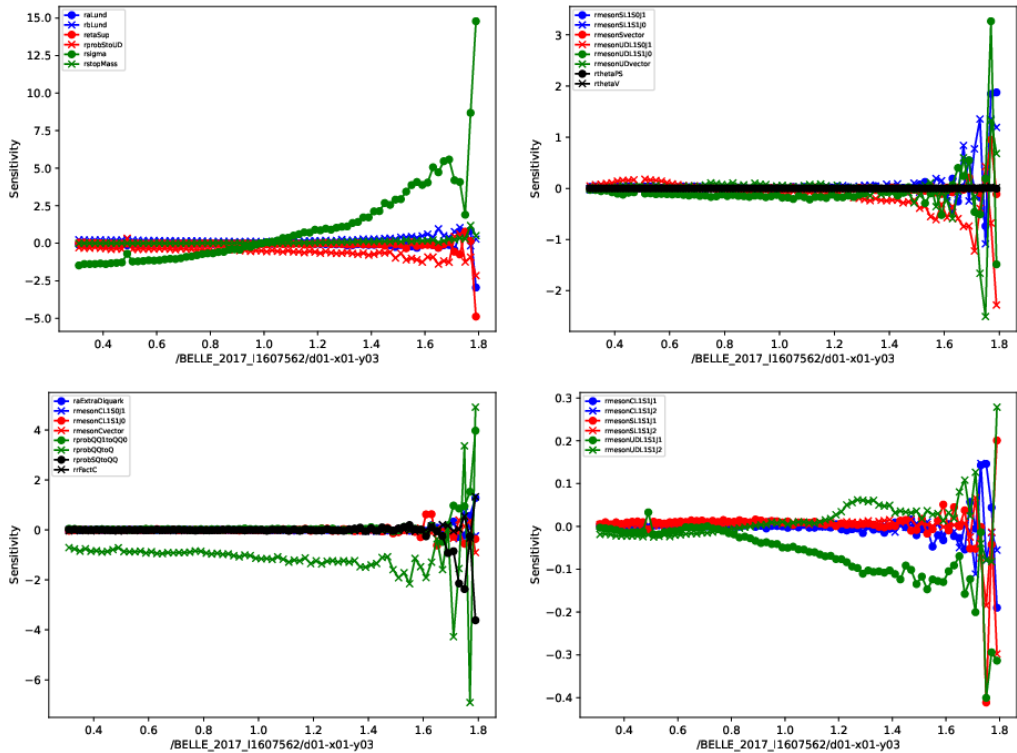


Figure 13: Sensitivities of the $\pi^+\pi^-$ cross sections as a function of the invariant mass, in the z bin. The different curves correspond to the sensitivities to the various tune parameters.

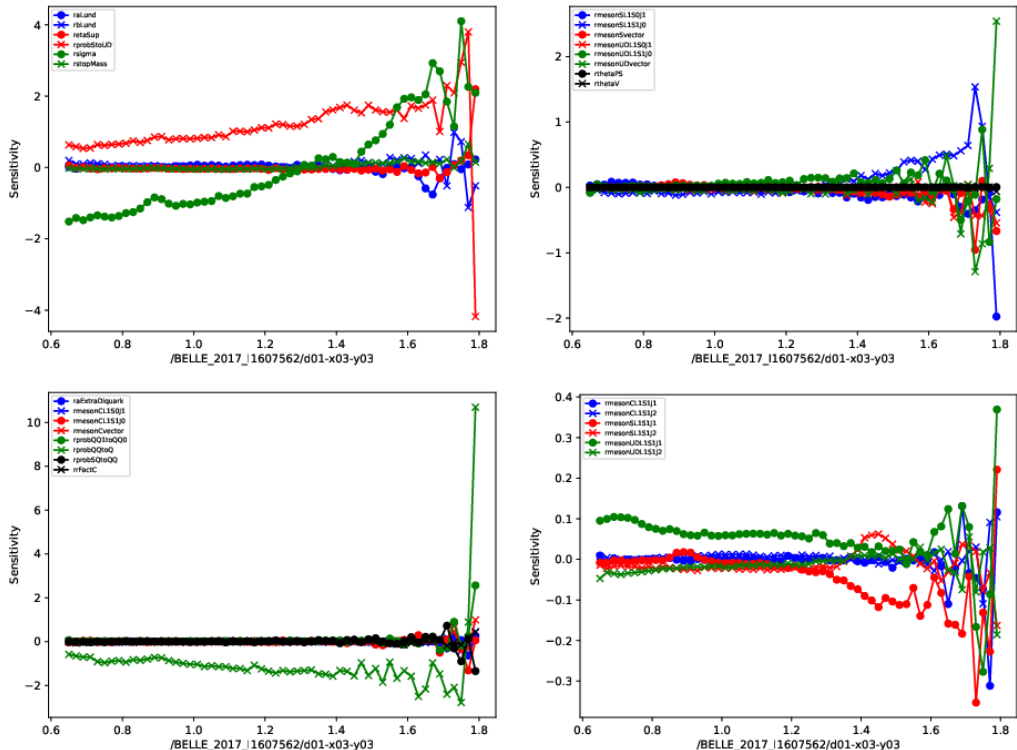


Figure 14: Sensitivities of the π^+K^- cross sections as a function of the invariant mass, in the z bin. The different curves correspond to the sensitivities to the various tune parameters.

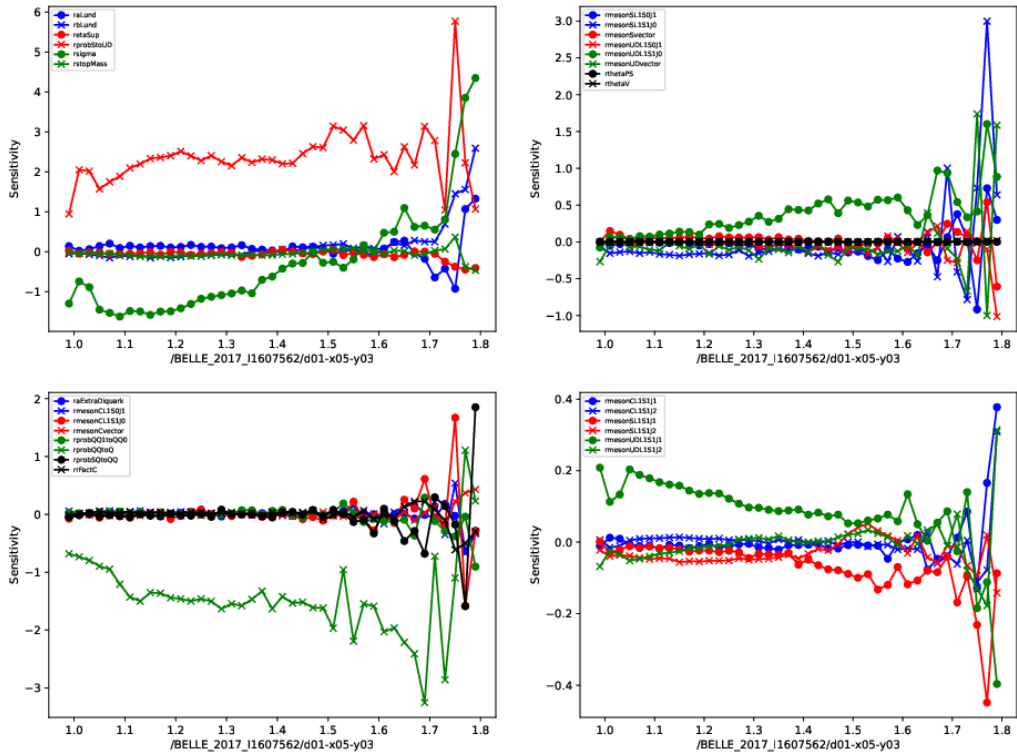


Figure 15: Sensitivities of the K^+K^- cross sections as a function of the invariant mass, in the z bin. The different curves correspond to the sensitivities to the various tune parameters.

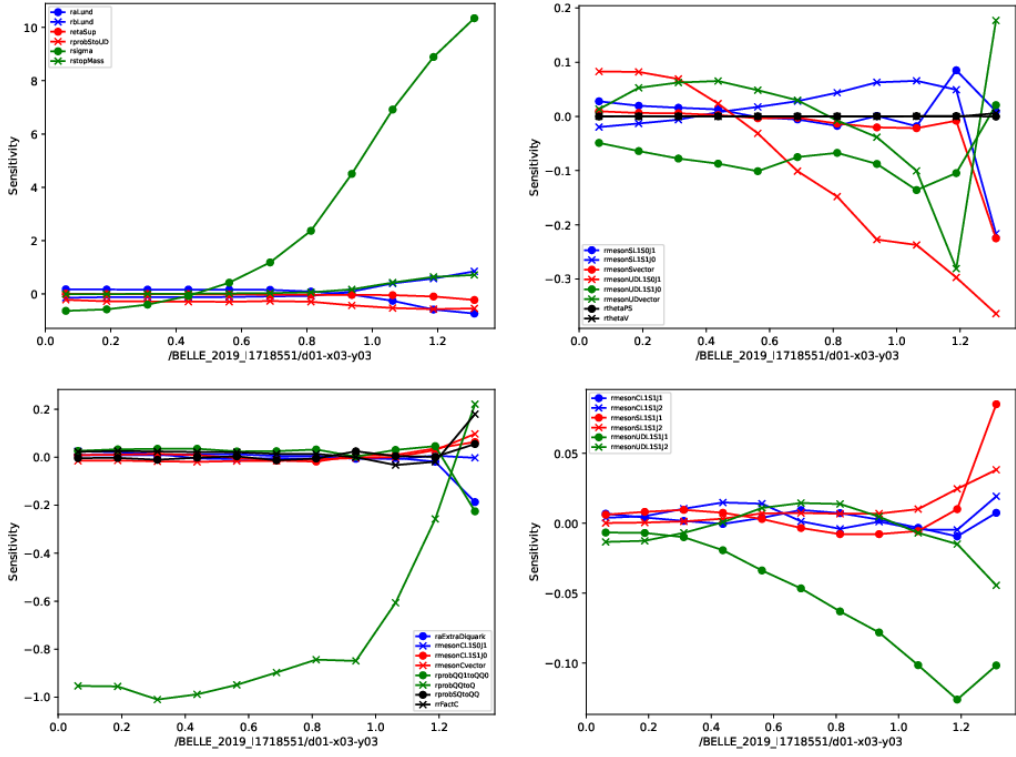


Figure 16: Sensitivities of the π cross sections as a function of the transverse momentum in the z bin and a thrust value of $0.8 - 0.9$. The different curves correspond to the sensitivities to the various tune parameters.

448 be seen in Figs. 16 to 18.

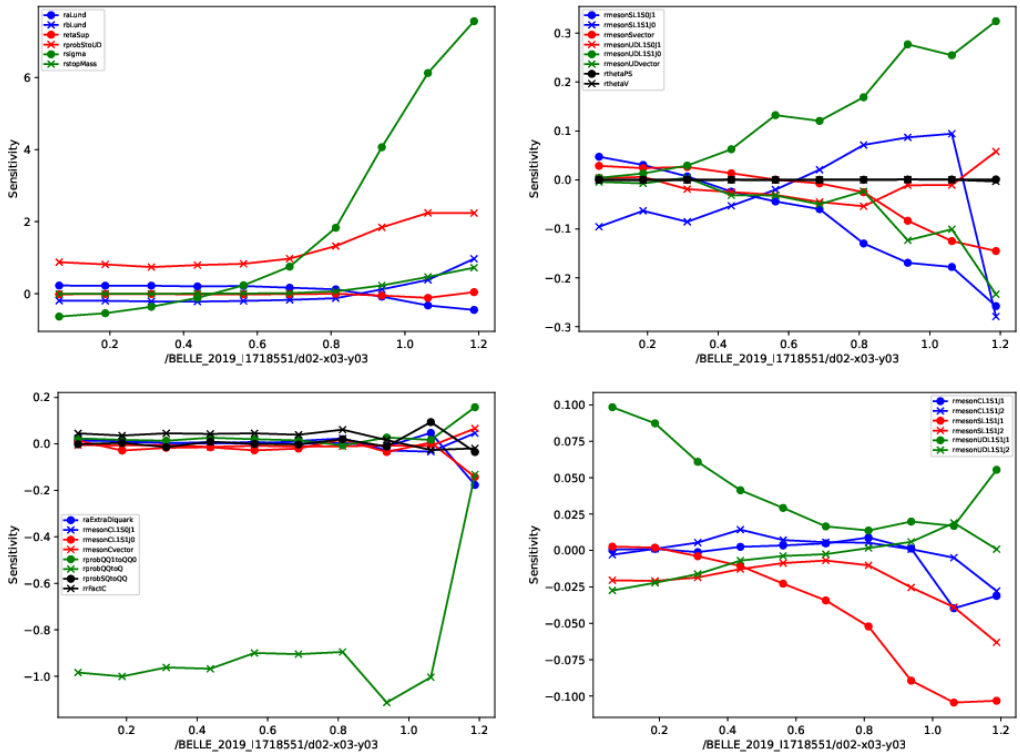


Figure 17: Sensitivities of the π cross sections as a function of the transverse momentum in the z bin and a thrust value of $0.8 - 0.9$. The different curves correspond to the sensitivities to the various tune parameters.

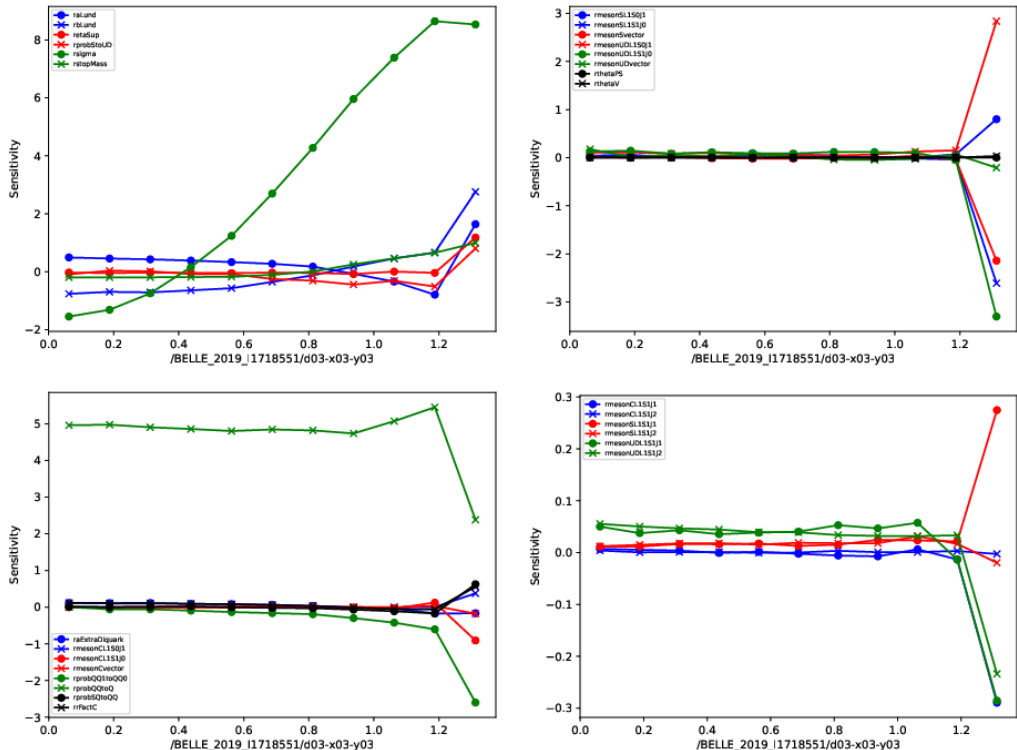


Figure 18: Sensitivities of the π cross sections as a function of the transverse momentum in the z bin and a thrust value of $0.8 - 0.9$. The different curves correspond to the sensitivities to the various tune parameters.

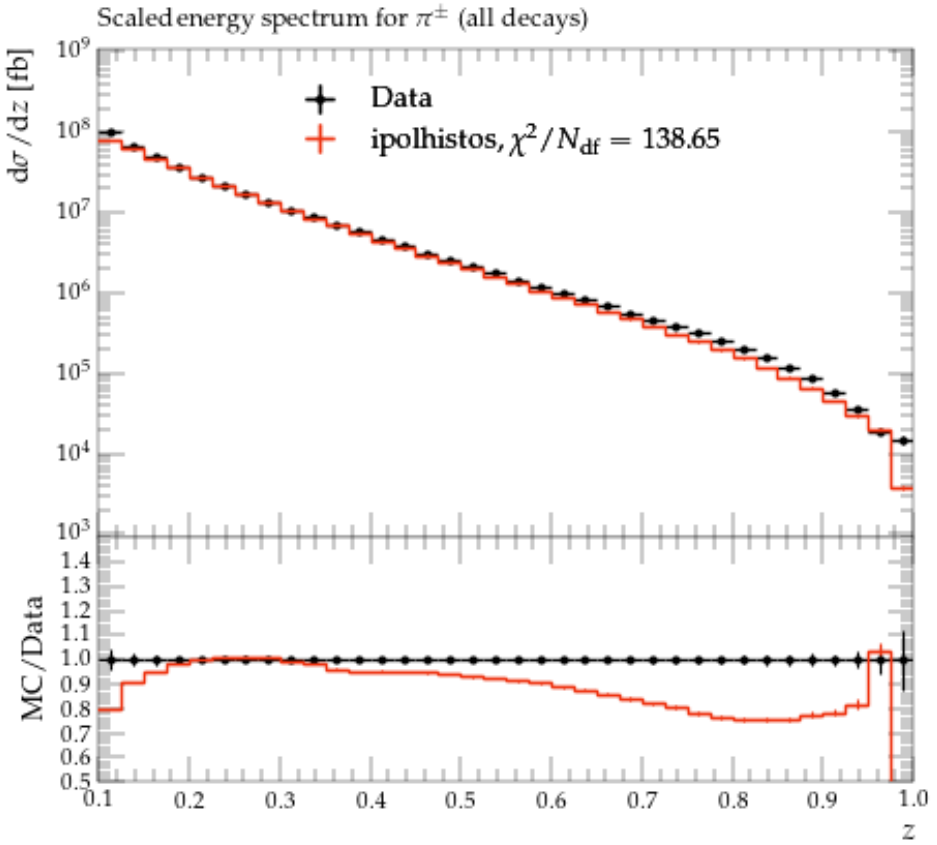


Figure 19: Pion cross sections as a function of the fractional energy z . The data is displayed by black points while the best fit result in red.

449 7 Tuning fits

450 7.1 Main hadrons

451 The best results can be seen in Fig. 19 to 21 for the main pion, kaon and proton
 452 cross sections. One can see that for the mesons the data can be described reasonably
 453 well overall, while the high precision of the pion data still results in fairly high χ^2 .
 454 The proton data cannot be described so well which appears to be a common problem
 455 for baryon production in the Lund model as will be apparent from the other baryon
 456 related results below.

457 7.2 Decaying and charmed mesons

458 For the various light mesons that were studied in publication [3], the tuning efforts
 459 are able to provide a good description of the data and generally low χ^2 . Those fit
 460 results are displayed in Figs. 22 to 25.

461 Charmed mesons are also mostly well described, with the vector mesons compar-
 462 ing particularly well, as can be seen in Figs. 26 to 28. On the strange D mesons are
 463 slightly less well described as apparently the additional shift in the peak positions
 464 due to the heavier strange quarks cannot be well accommodated in the Lund model.

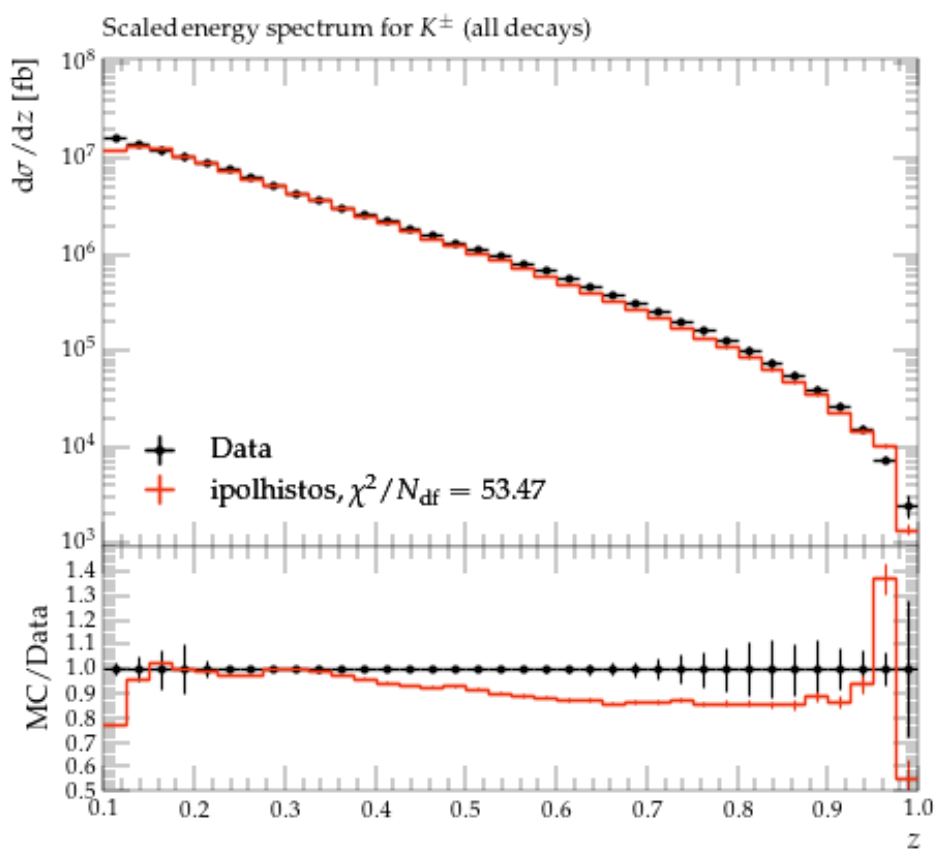


Figure 20: Kaon cross sections as a function of the fractional energy z . The data is displayed by black points while the best fit result in red.

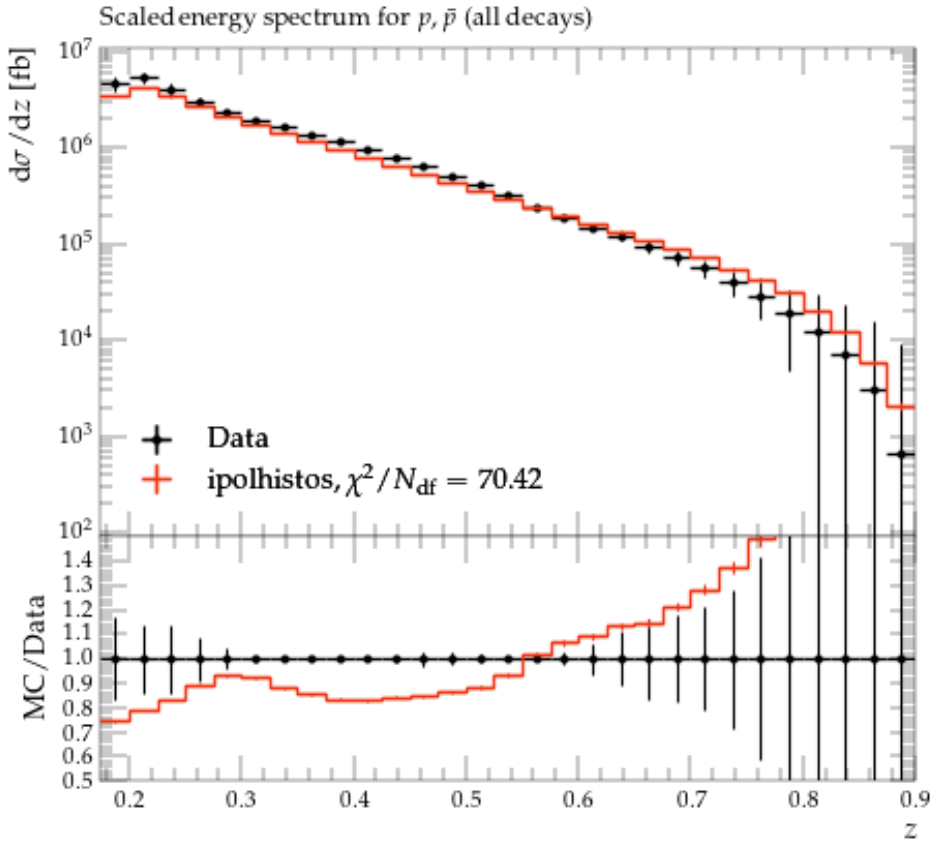


Figure 21: Proton cross sections as a function of the fractional energy z . The data is displayed by black points while the best fit result in red.

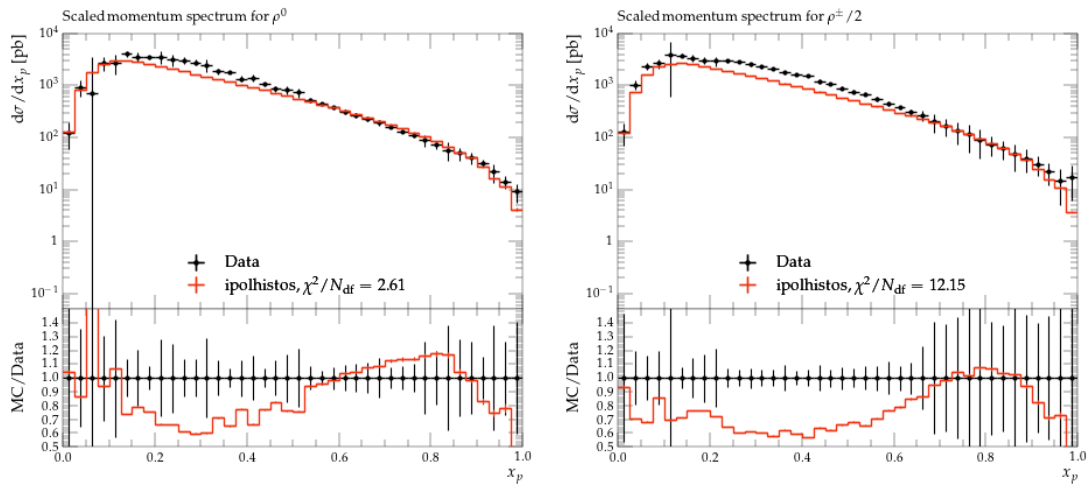


Figure 22: Left: neutral ρ cross sections as a function of the fractional momentum x_p . Right: charged ρ cross sections. The data is displayed by black points while the best fit result in red.

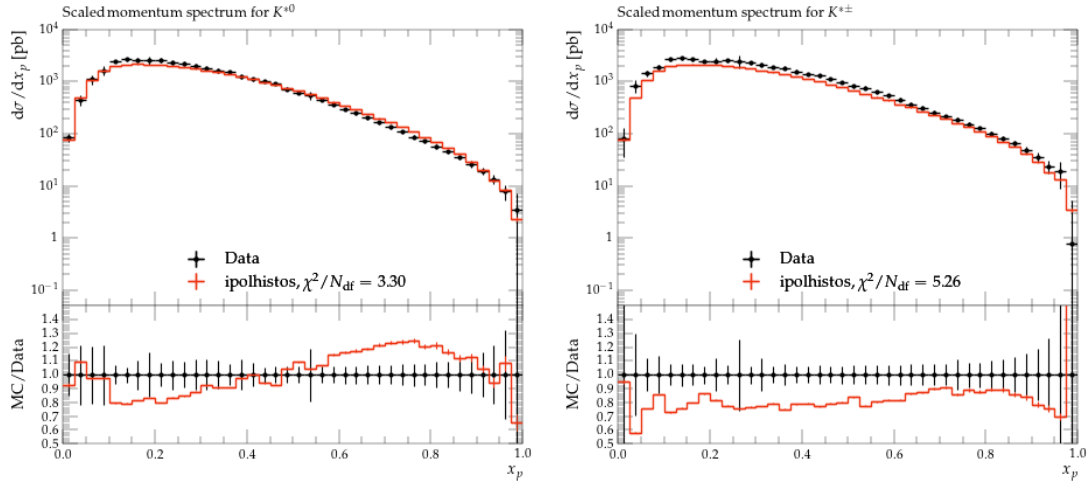


Figure 23: Left: neutral K^* cross sections as a function of the fractional momentum x_p . Right: charged K^* cross sections. The data is displayed by black points while the best fit result in red.

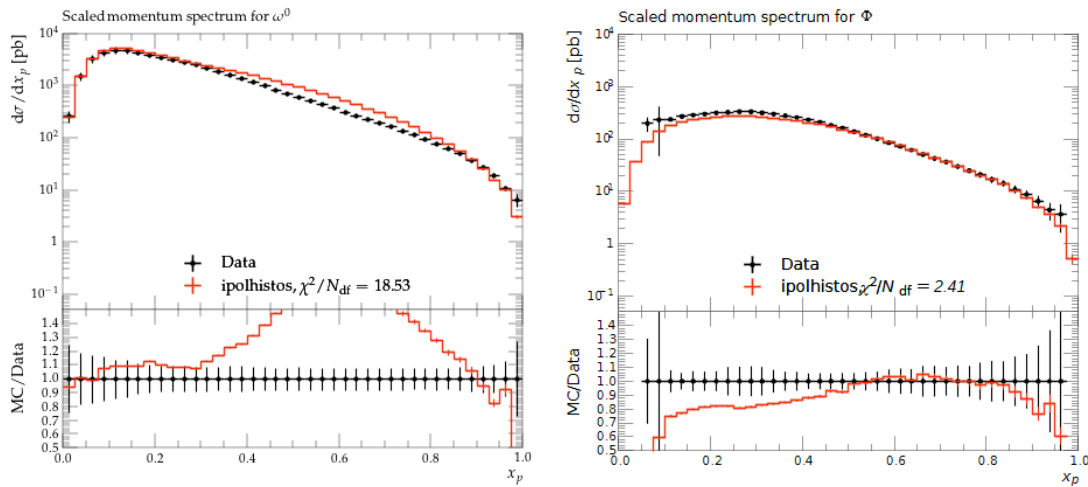


Figure 24: Left: ω cross sections as a function of the fractional momentum x_p . Right: ϕ cross sections. The data is displayed by black points while the best fit result in red. The missing χ^2 is 3.96.

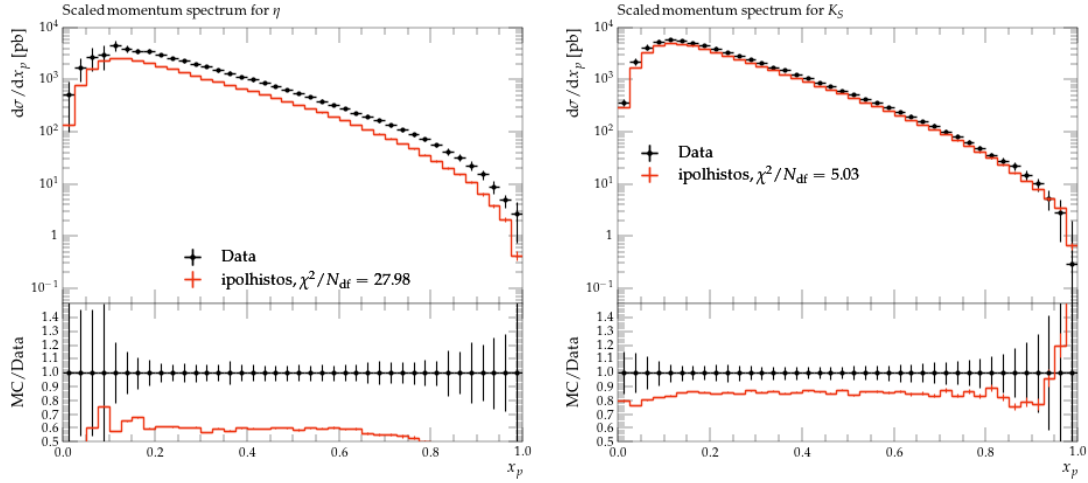


Figure 25: Left: η cross sections as a function of the fractional momentum x_p . Right: K_S cross sections. The data is displayed by black points while the best fit result in red.

465 In the figures the χ^2 values are often given as nans, since Rivet cannot deal with
 466 empty bins, but they were added by hand based on the professor tuning outcome
 467 which does provide them correctly.

468 7.3 Di-hadrons in various configurations

469 In the following, examples of the dihadron invariant mass distributions are shown
 470 for one low and one higher fractional energy bin in Figs. 29 to 34. One can see that
 471 for many hadron combinations, the overall description is good, but some features
 472 are not well reproduced. Most notably in the opposite-sign pion-kaon spectra the
 473 bump at around 1.5 GeV is not as pronounced in the MC, or rather somewhat
 474 elongated in comparison to the data. As the underlying decay of D mesons into
 475 $K\pi\pi$ is also present in PYTHIA, likely some of the details are not as well described
 476 there compared to EvtGen (as the bump was very clearly visible in the Belle I MC
 477 as well). Another aspect that is not well described are the same-sign pion pair's low
 478 mass region which generally underestimates the amount of pairs. For pion-kaon and
 479 kaon pairs the description is generally quite resonable also at lower masses.

480 Also the back-to-back di-hadron distributions as a function of fractional energies,
 481 the description of the data by the best tune is again very reasonable, as shown in
 482 Figs. 35 to 40 for selected fractional energy bin and hadron type combinations.

483 7.4 Transverse momentum dependent cross sections

484 The transverse momentum dependent cross sections are also fairly well described,
 485 particularly the low transverse momentum region that most directly is sensitive to
 486 the transverse momentum generated in the fragmentation process. In the higher
 487 transverse momentum tails, some slight differences can be seen, albeit with rather
 488 large uncertainties on the measurements.

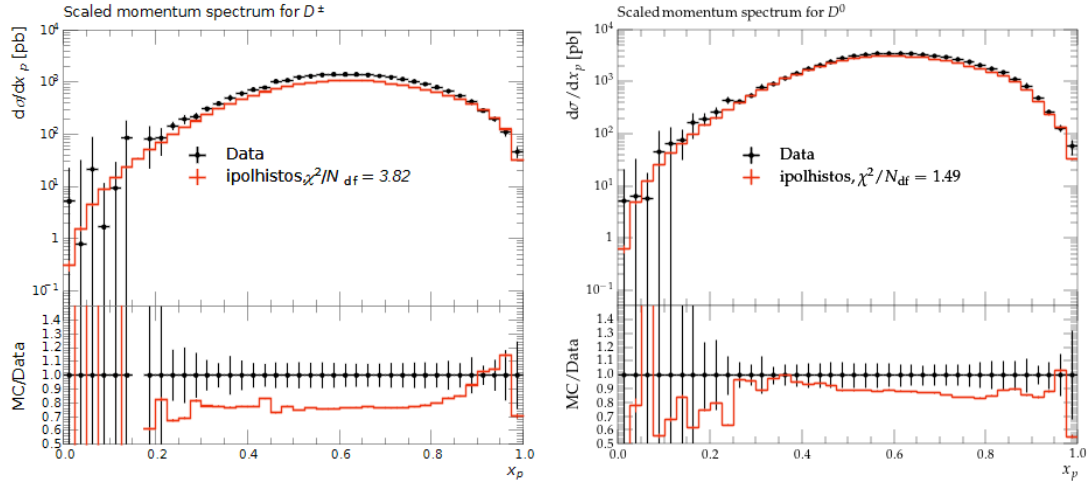


Figure 26: Left: D^+ cross sections as a function of the fractional momentum x_p . Right: D^0 cross sections. The data is displayed by black points while the best fit result in red.

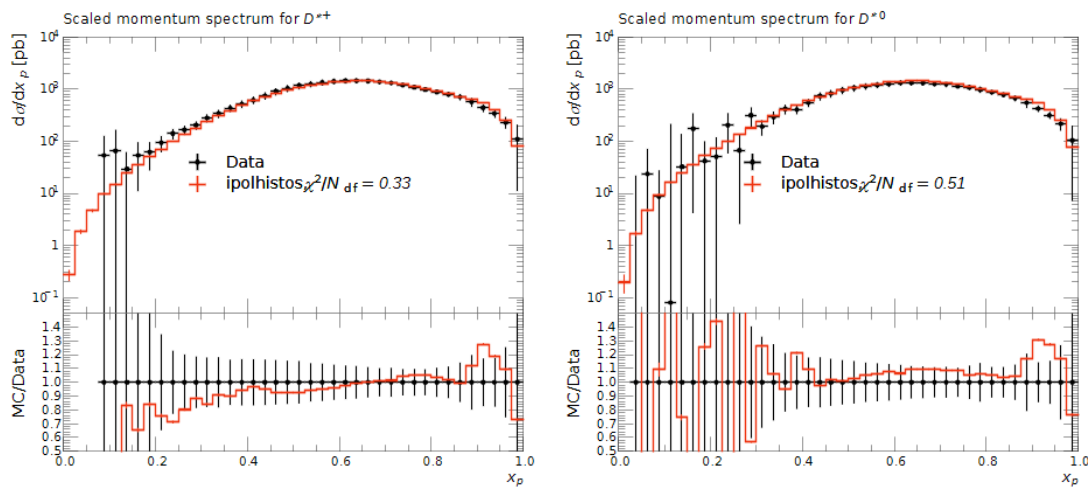


Figure 27: Left: D^{*+} cross sections as a function of the fractional momentum x_p . Right: D^{*0} cross sections. The data is displayed by black points while the best fit result in red.

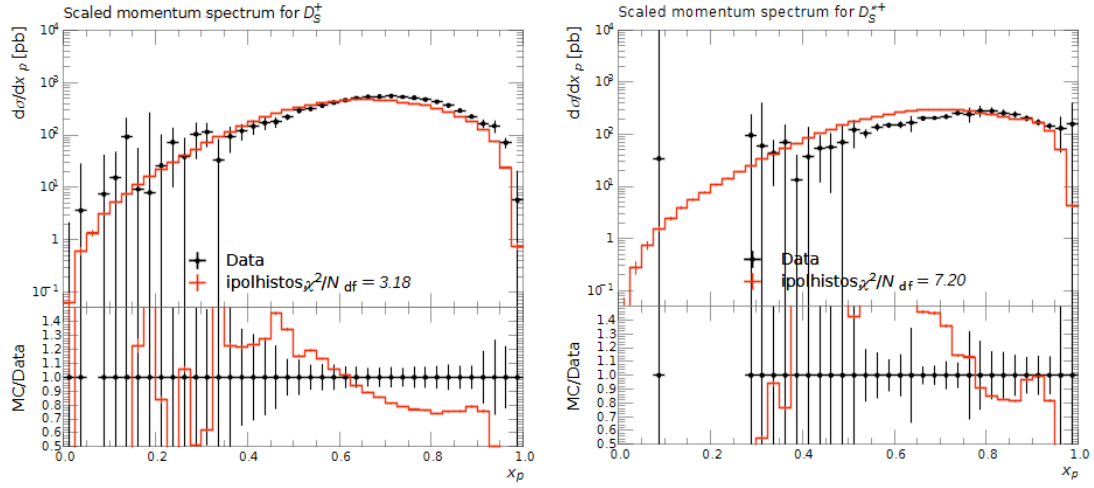


Figure 28: Left: D_s^+ cross sections as a function of the fractional momentum x_p . Right: D_s^{*+} cross sections. The data is displayed by black points while the best fit result in red.

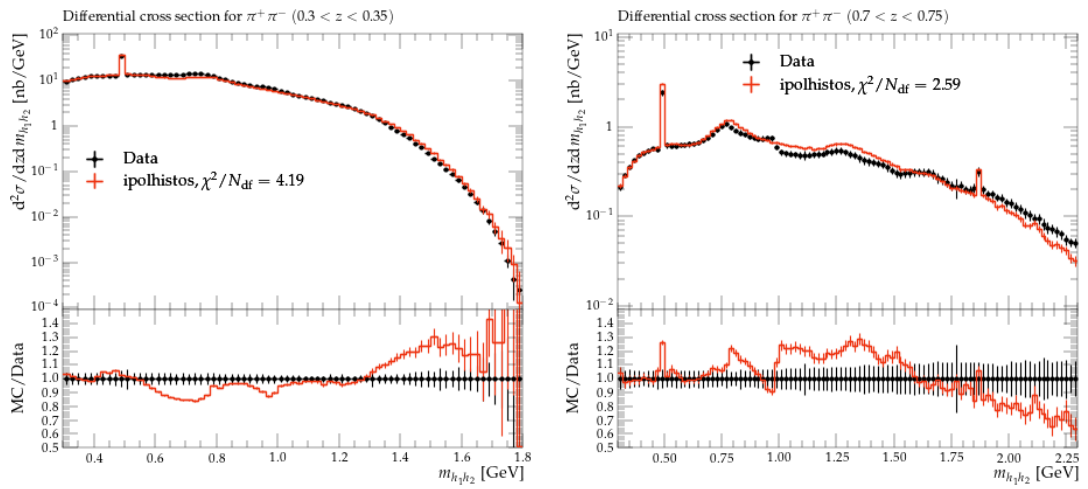


Figure 29: Left: $\pi^+\pi^-$ pair cross sections as a function of the invariant mass m for the fractional energy bin $0.3 - 0.35$. Right: The same for the fractional energy bin $0.7 - 0.75$. The data is displayed by black points while the best fit result in red.

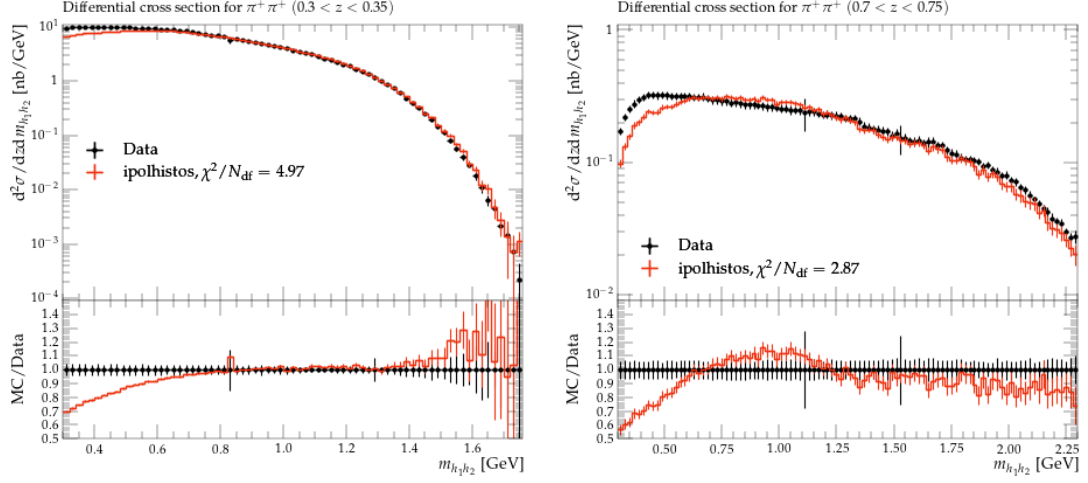


Figure 30: Left: $\pi^+\pi^+$ pair cross sections as a function of the invariant mass m for the fractional energy bin $0.3 - 0.35$. Right: The same for the fractional energy bin $0.7 - 0.75$. The data is displayed by black points while the best fit result in red.

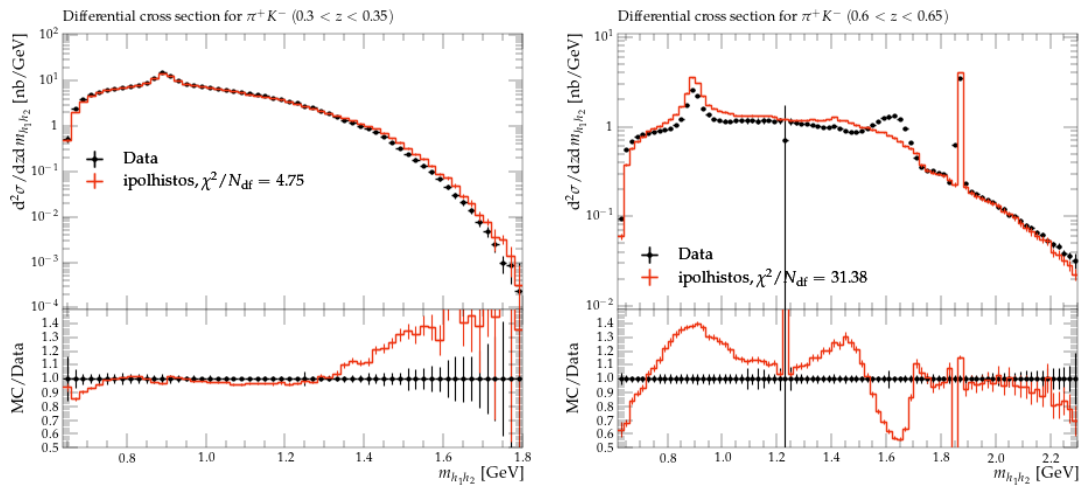


Figure 31: Left: π^+K^- pair cross sections as a function of the invariant mass m for the fractional energy bin $0.3 - 0.35$. Right: The same for the fractional energy bin $0.6 - 0.65$. The data is displayed by black points while the best fit result in red.

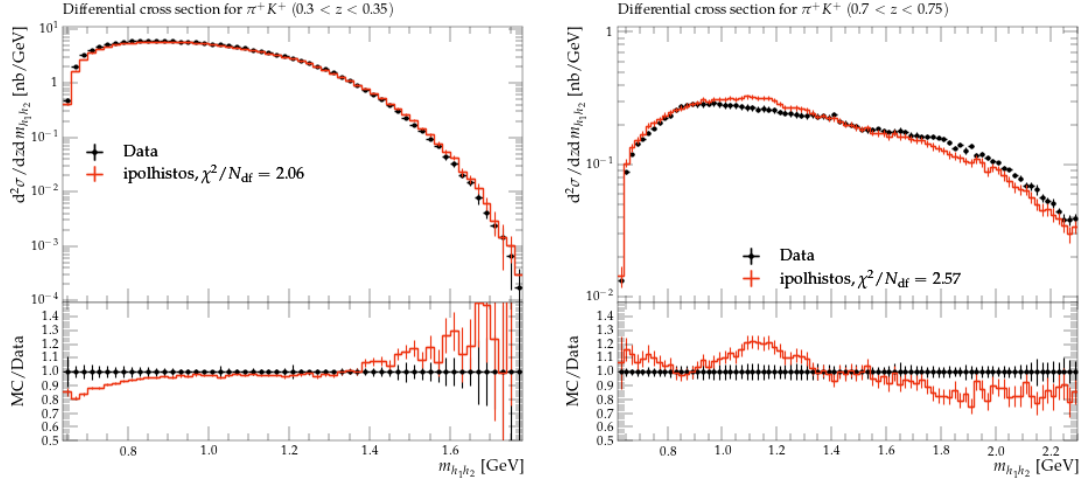


Figure 32: Left: π^+K^+ pair cross sections as a function of the invariant mass m for the fractional energy bin $0.3 - 0.35$. Right: The same for the fractional energy bin $0.7 - 0.75$. The data is displayed by black points while the best fit result in red.

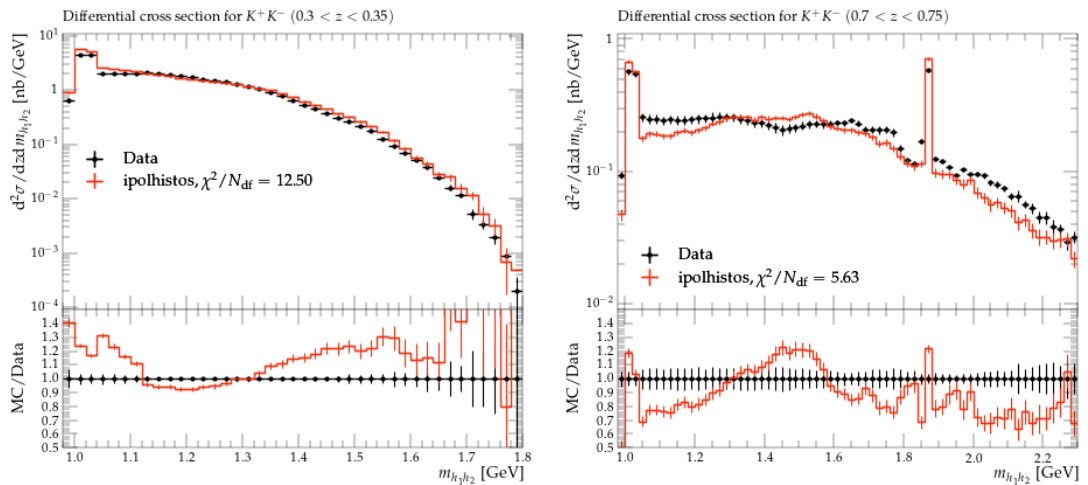


Figure 33: Left: K^+K^- pair cross sections as a function of the invariant mass m for the fractional energy bin $0.3 - 0.35$. Right: The same for the fractional energy bin $0.7 - 0.75$. The data is displayed by black points while the best fit result in red.

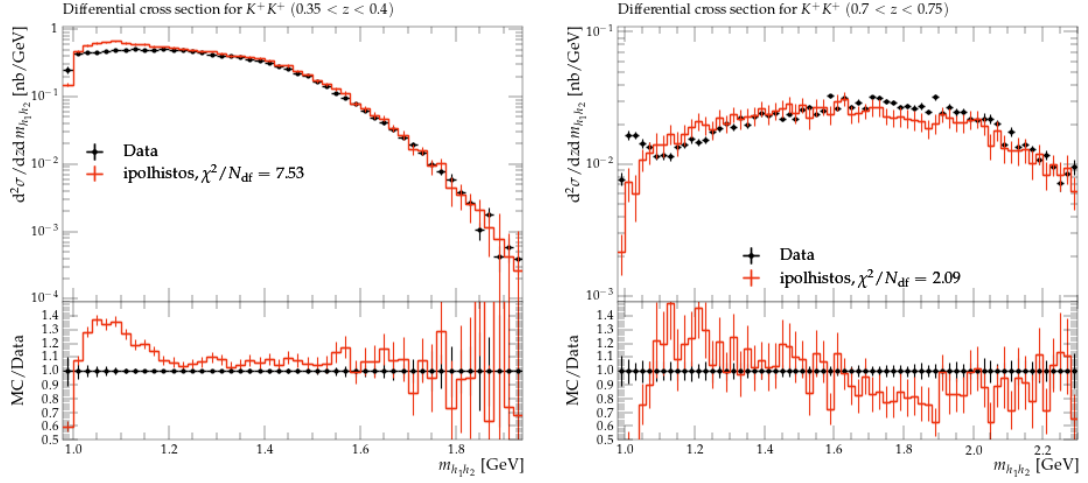


Figure 34: Left: K^+K^+ pair cross sections as a function of the invariant mass m for the fractional energy bin $0.35 - 0.4$. Right: The same for the fractional energy bin $0.7 - 0.75$. The data is displayed by black points while the best fit result in red.

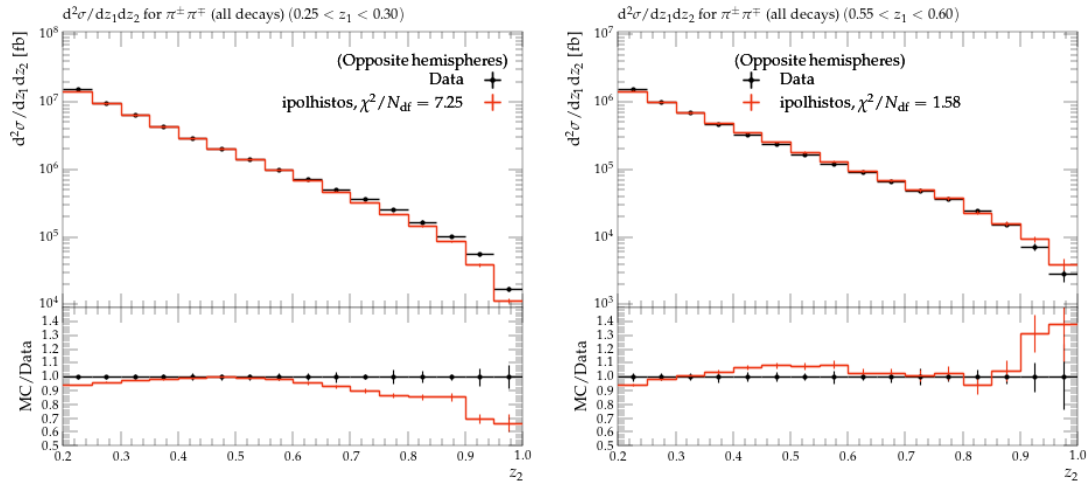


Figure 35: Left: $\pi^+\pi^-$ pair cross sections in opposite hemispheres as a function of the invariant mass z_2 for the fractional energy bin $0.25 < z_1 < 0.3$. Right: The same for the fractional energy bin $0.55 < z_1 < 0.6$. The data is displayed by black points while the best fit result in red.

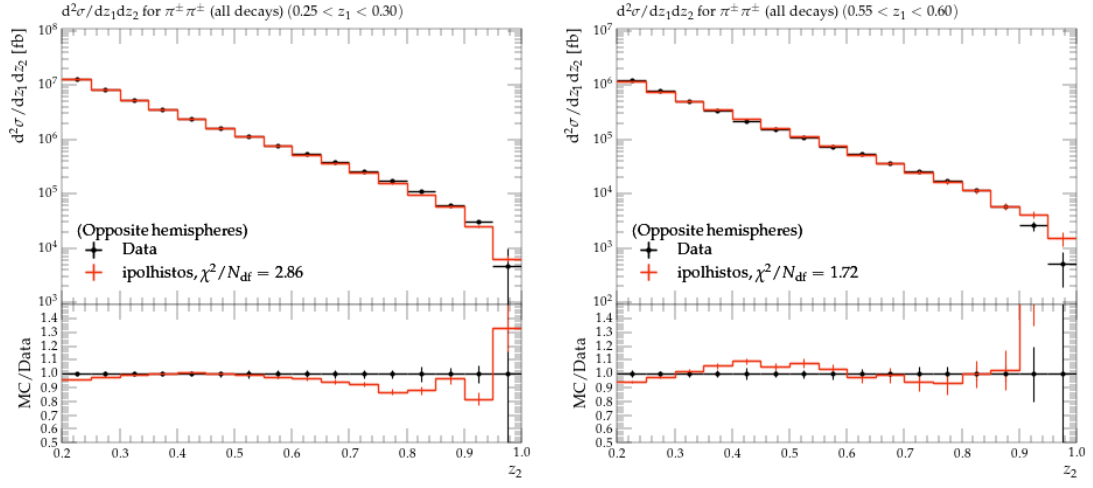


Figure 36: Left: $\pi^+\pi^+$ pair cross sections in opposite hemispheres as a function of the invariant mass z_2 for the fractional energy bin $0.25 < z_1 < 0.3$. Right: The same for the fractional energy bin $0.55 < z_1 < 0.6$. The data is displayed by black points while the best fit result in red.

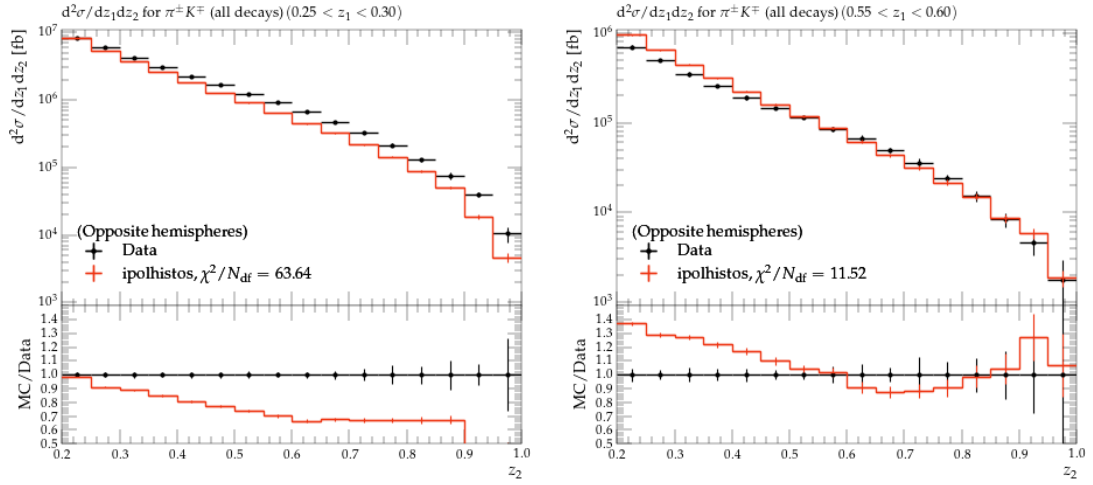


Figure 37: Left: π^+K^- pair cross sections in opposite hemispheres as a function of the invariant mass z_2 for the fractional energy bin $0.25 < z_1 < 0.3$. Right: The same for the fractional energy bin $0.55 < z_1 < 0.6$. The data is displayed by black points while the best fit result in red.

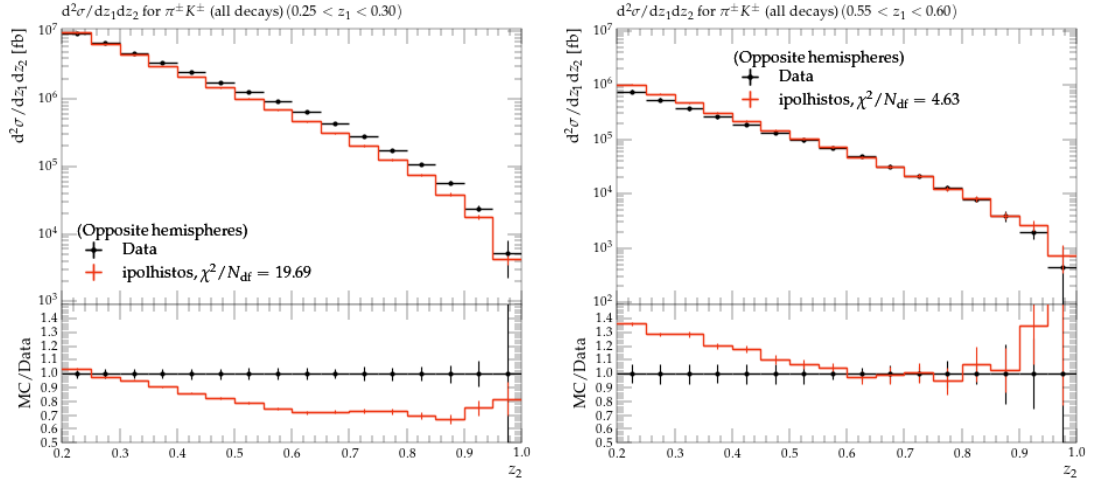


Figure 38: Left: $\pi^+ K^+$ pair cross sections in opposite hemispheres as a function of the invariant mass z_2 for the fractional energy bin $0.25 < z_1 < 0.3$. Right: The same for the fractional energy bin $0.55 < z_1 < 0.6$. The data is displayed by black points while the best fit result in red.

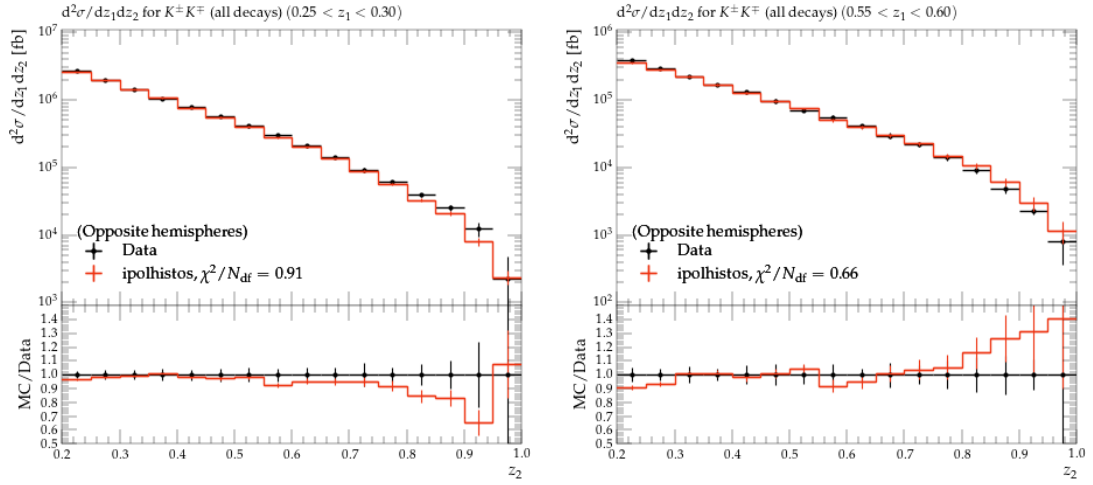


Figure 39: Left: $K^+ K^-$ pair cross sections in opposite hemispheres as a function of the invariant mass z_2 for the fractional energy bin $0.25 < z_1 < 0.3$. Right: The same for the fractional energy bin $0.55 < z_1 < 0.6$. The data is displayed by black points while the best fit result in red.

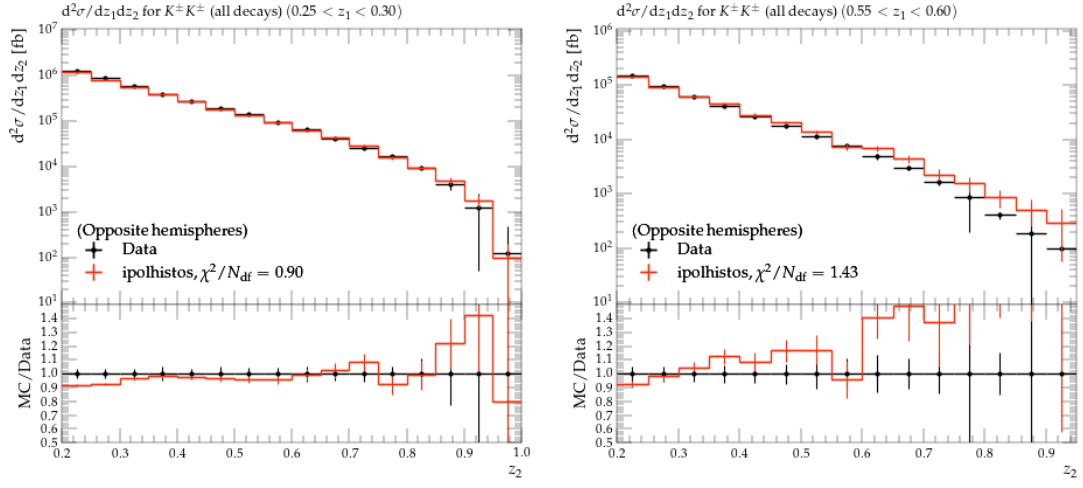


Figure 40: Left: K^+K^- pair cross sections in opposite hemispheres as a function of the invariant mass z_2 for the fractional energy bin $0.25 < z_1 < 0.3$. Right: The same for the fractional energy bin $0.55 < z_1 < 0.6$. The data is displayed by black points while the best fit result in red.

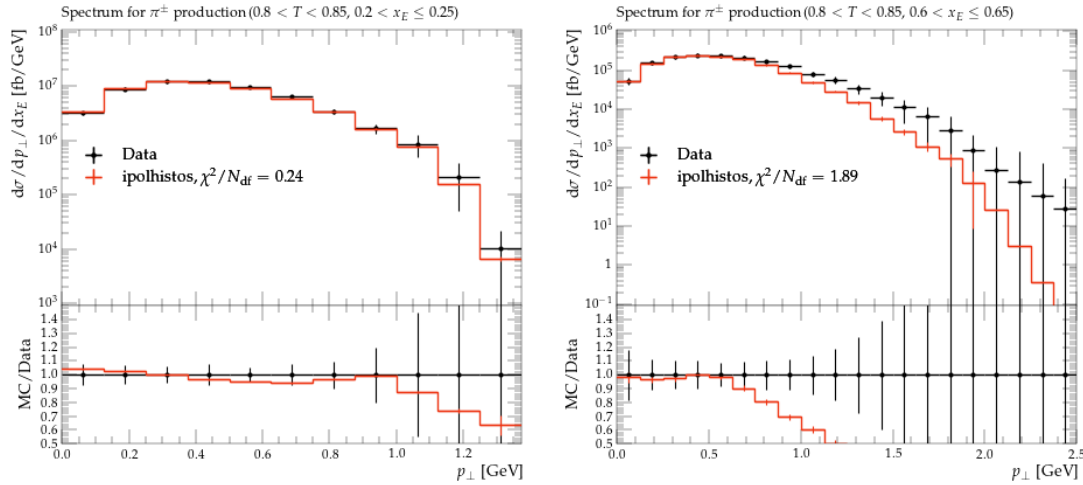


Figure 41: Left: π^\pm cross sections as a function of the transverse momentum p_T for the fractional energy bin $0.2 < z_1 < 0.25$ in the thrust bin $0.8 - 0.9$. Right: The same for the fractional energy bin $0.6 < z_1 < 0.65$. The data is displayed by black points while the best fit result in red.

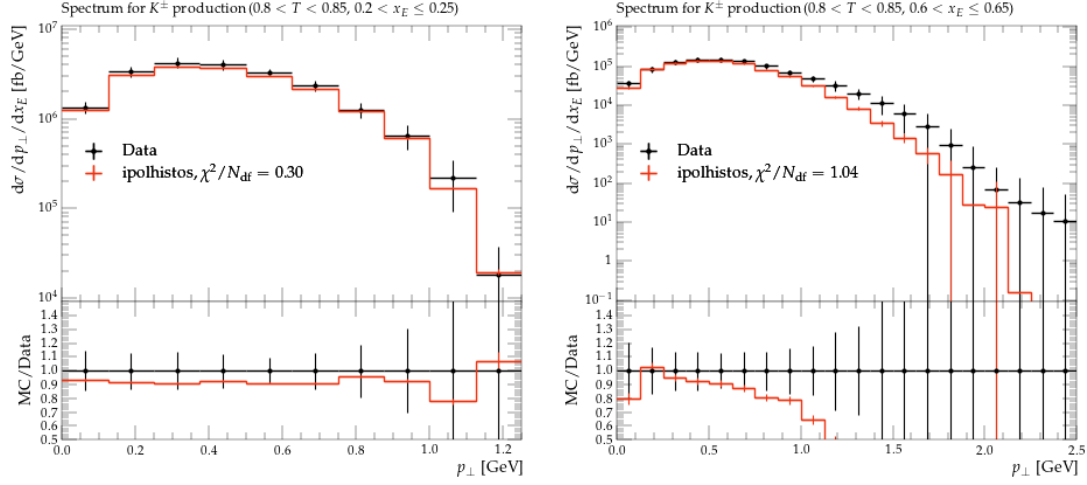


Figure 42: Left: K^\pm cross sections as a function of the transverse momentum p_T for the fractional energy bin $0.2 < z_1 < 0.25$ in the thrust bin $0.8 - 0.9$. Right: The same for the fractional energy bin $0.6 < z_1 < 0.65$. The data is displayed by black points while the best fit result in red.

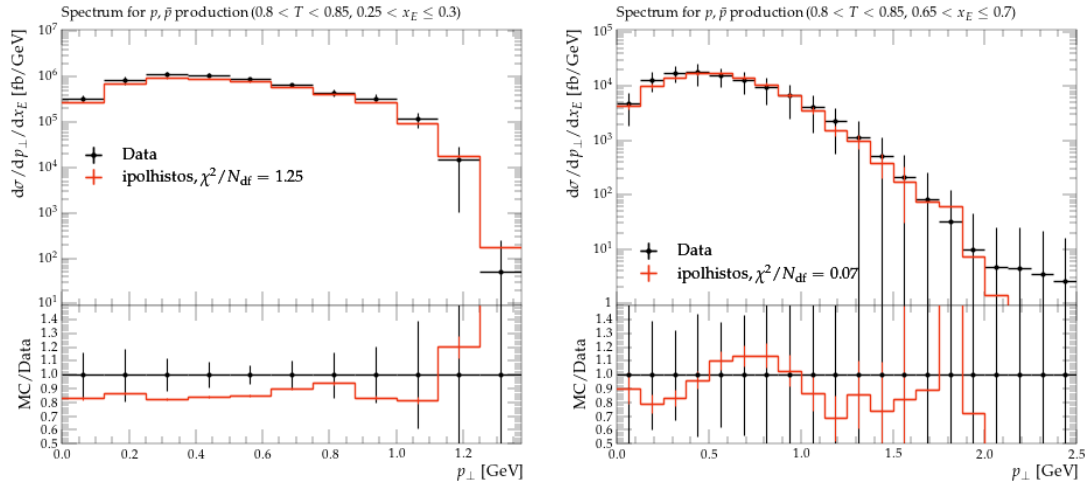


Figure 43: Left: p cross sections as a function of the transverse momentum p_T for the fractional energy bin $0.2 < z_1 < 0.25$ in the thrust bin $0.8 - 0.9$. Right: The same for the fractional energy bin $0.6 < z_1 < 0.65$. The data is displayed by black points while the best fit result in red.

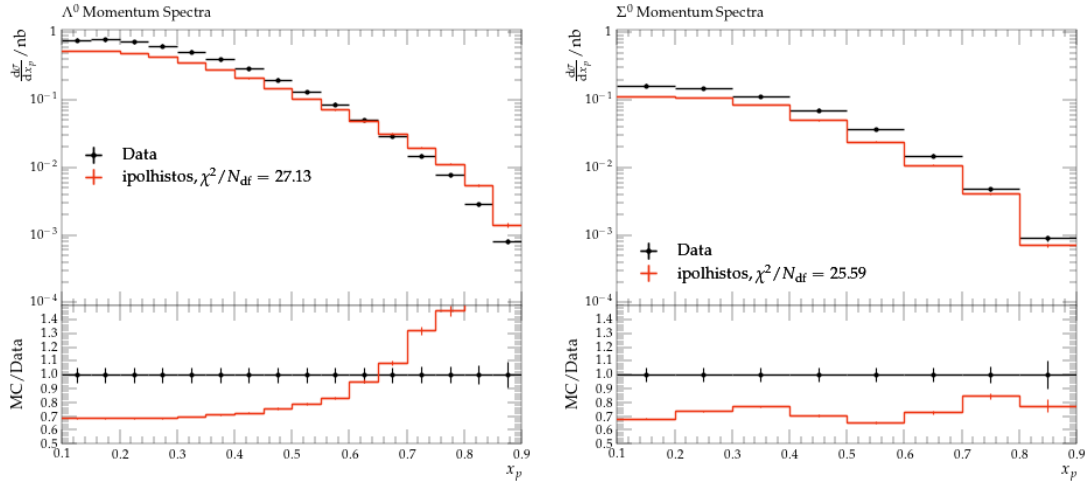


Figure 44: Left: Λ spectrum as a function of x_p . Right Σ^0 spectrum as a function of x_p . The data is displayed by black points while the best fit result in red.

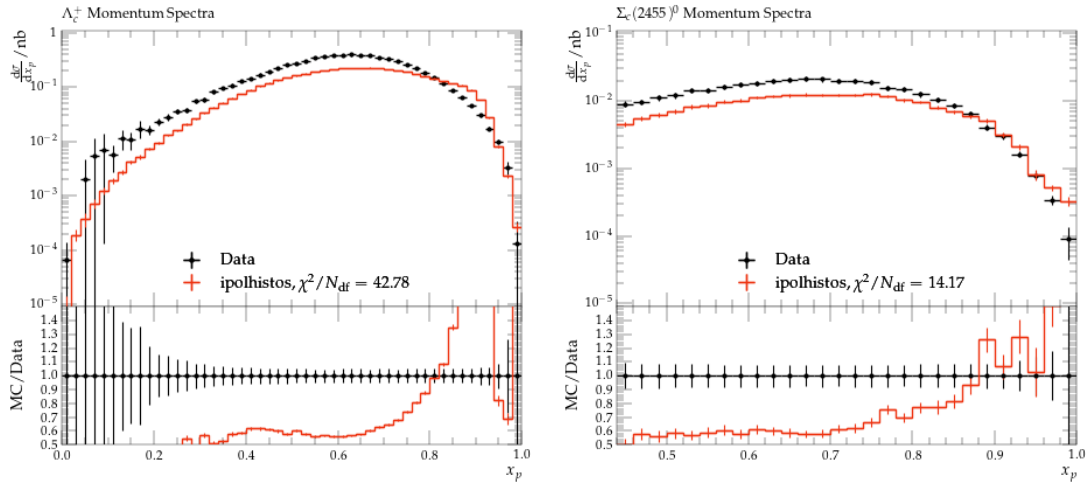


Figure 45: Left: Λ_c^+ spectrum as a function of x_p . Right $\Sigma_c(2455)^0$ spectrum as a function of x_p . The data is displayed by black points while the best fit result in red.

489 7.5 Hyperons and charmed baryons

490 For hyperons the description is still not as good, even after including the popcorn
 491 variables and used the bug-fixed version of PYTHIA. The overall shapes do have
 492 improved, however, as can be seen in Figs. 44 and 45 for some hyperons and charmed
 493 baryons, respectively. The peak position of the charmed baryons is somewhat similar
 494 to the measurements, but the tune predicts a rather abrupt drop-off of the cross
 495 sections at very high momentum fractions that is not confirmed in the data, or at
 496 least not as sharp.

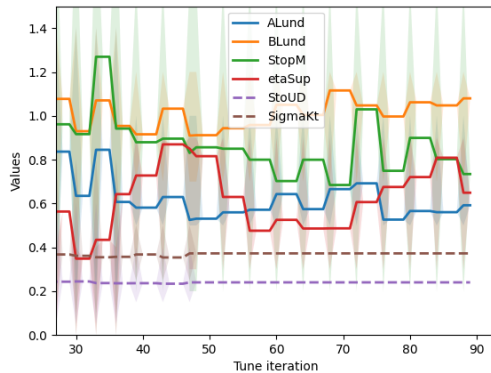


Figure 46: Main Lund variables, the allowed ranges are shown in shaded regions and the best values as a function of the various tuning iterations

497 8 Systematic uncertainties and tests

498 The best variables and their variations are summarized in Table 2 in comparison to
 499 the default values of PYTHIA. In this table the best values are given in the second
 500 column, the lower and upper values represent the lowest and highest variations of
 501 the tune iterations to the best value (i.e. the last iteration for that particular vari-
 502 able). The variations are just given as a measure of how much these variables varied
 503 during the tuning evaluations and cannot be considered as reliable uncertainties. In
 504 turn, the statistical uncertainties from the tuning efforts are tiny and are therefore
 505 not tabulated. One can see that the variables that have been retired after several
 506 iterations were quite stable. The individual sets of variables and their variations are
 507 also visualized in the following figures as a function of their iterations. The Main
 508 Lund string fragmentation variables can be found in Fig. 46. One sees again that
 509 the strangeness suppression and the transverse momentum generation are indeed
 510 not changing much over the iterations.

511 The light quark vector meson and higher spin variables can be seen in Fig. 47.
 512 Especially the higher spin variables are not particularly well determined and thus
 513 fluctuate from iteration to iteration, but the vector meson fraction is fairly stable
 514 which is why it was fixed eventually.

515 The corresponding strange and charm variables are displayed in Figs. 48 and 49,
 516 respectively. In these, one can see that the two vector mesons fractions are again
 517 the most stable variables and that the charm vector meson fraction is significantly
 518 larger than that of strange quarks which again is slightly larger than that for light
 519 quarks. The higher spin values typically vary much as well.

520 The baryon related fragmentation variables are displayed in Fig. 50. Apart from
 521 the main diquark fragmentation and the extra Lund factor for diquarks, the values
 522 are fluctuating significantly between iterations. After the inclusion of the popcorn
 523 values, the vector diquark fraction also appears to stabilize.

524 The vector and pseudoscalar mixing angles are displayed in Fig. 51. Especially
 525 the pseudoscalar mixing value is fluctuating significantly while the vector angle is
 526 slightly more stable.

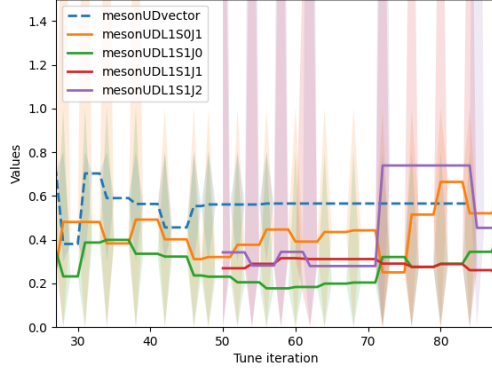


Figure 47: Light quark related vector meson and higher spin variables as a function of the various tuning iterations, the allowed ranges are shown in shaded regions and the best values as the center line. Dashed lines represent variables that have been fixed after they became stable.

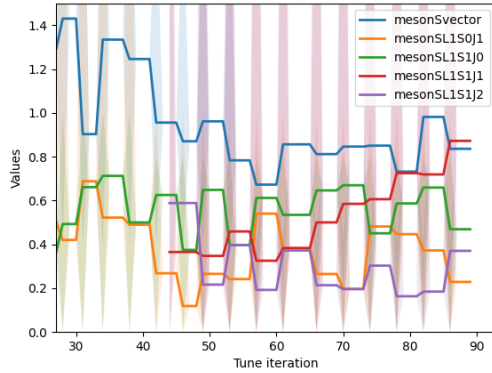


Figure 48: Strange quark related vector meson and higher spin variables as a function of the various tuning iterations, the allowed ranges are shown in shaded regions and the best values as the center line. Dashed lines represent variables that have been fixed after they became stable.

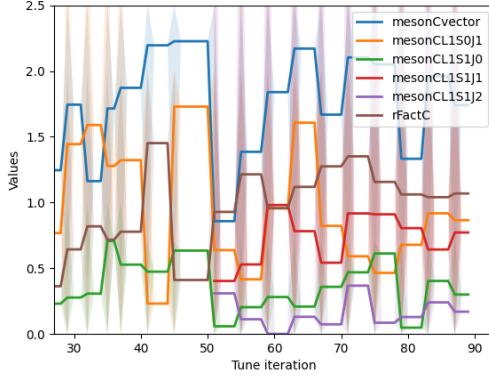


Figure 49: Charm quark related vector meson and higher spin variables as a function of the various tuning iterations, the allowed ranges are shown in shaded regions and the best values as the center line. Dashed lines represent variables that have been fixed after they became stable.

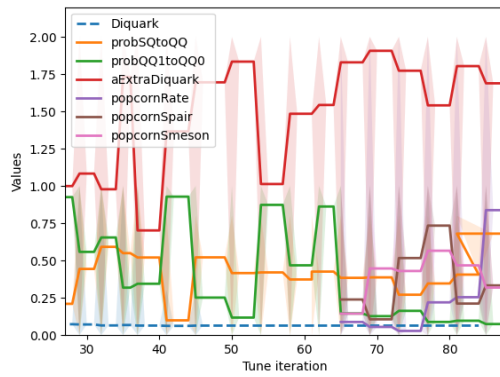


Figure 50: Baryon related variables as a function of the various tuning iterations, the allowed ranges are shown in shaded regions and the best values as the center line. Dashed lines represent variables that have been fixed after they became stable.

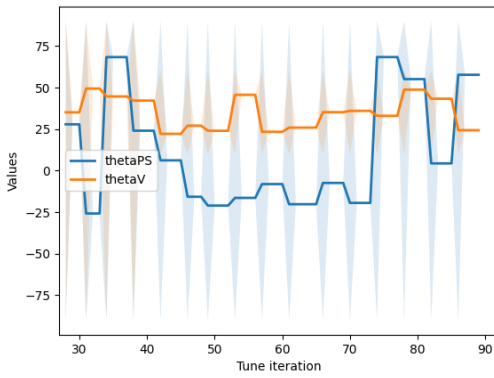


Figure 51: Mixing related variables as a function of the various tuning iterations, the allowed ranges are shown in shaded regions and the best values as the center line. Dashed lines represent variables that have been fixed after they became stable.

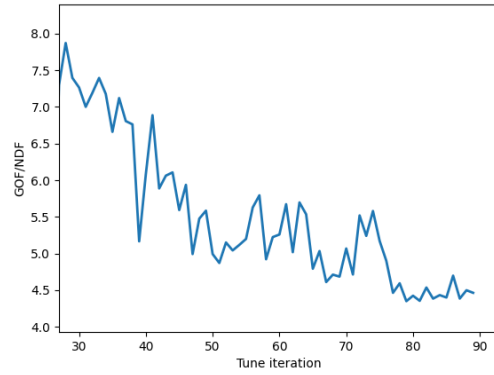


Figure 52: Evolution of the goodness of fit normalized by the number of degrees of freedom as a function of the various tuning iterations.

527 Last, the evolution of the goodness of fit as a function of the tune iterations is
 528 displayed in Fig. 52. One can generally see that the reduced χ^2 did decrease for the
 529 most part with the occasional fluctuations. After including the higher spin states
 530 and fixing some variables not too much improvement can be seen. Another reduction
 531 can be seen when including the popcorn variables at around tune iteration 65, but
 532 again after an initial drop the values flatten out. The last improvement can be seen
 533 from using the correct treatment of the extra a parameter that was fixed by the
 534 PYTHIA maintainers from iteration 77. Since then, the χ^2 does not improve anymore
 535 over two further iterations for each set of variables. This suggests that within the
 536 space of variables, no significant further improvements can be achieved and likely
 537 these are the best settings one can get.

538 8.1 Comparison to older settings

539 It is also instructive to learn how the different settings after tuning compare to
 540 the settings used as default or previously at Belle2. Those are displayed for vari-

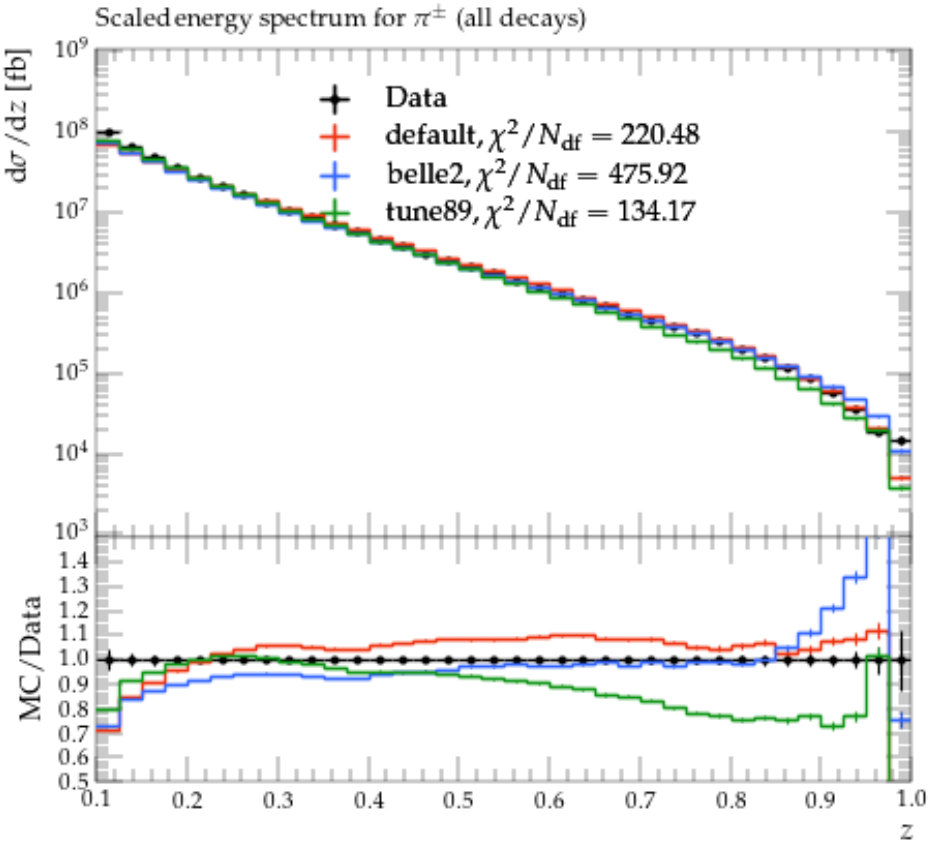


Figure 53: Pion cross sections as a function of the fractional energy z . The data is displayed by black points while the PYTHIA default is displayed in red, the current Belle2 setting in blue, and the best tune in green.

ous measurements in the figures 53 to 60. Due to some empty bins in the latest measurements which Rivet cannot handle well, the individual χ^2/NDF for these measurements are given as "nan". It is visible that while individual spectra for very abundant particles such as light mesons are often reasonably well-described by the older settings, especially di-hadron mass or momentum spectra and heavier particles can be much better described after tuning.

Summing up all other χ^2/NDF results gives average values of 15.3 for the Pythia default settings, 14.4 for the previously used Belle2 settings and 6.3 for the latest best settings. Note that these numbers are different from the actual fit numbers since here the average over all individual spectra is taken, rather than summing all points as is done in the fit. Those and the corresponding figures make it abundantly clear, that the tuning effort successfully improved the description of the included measurements.

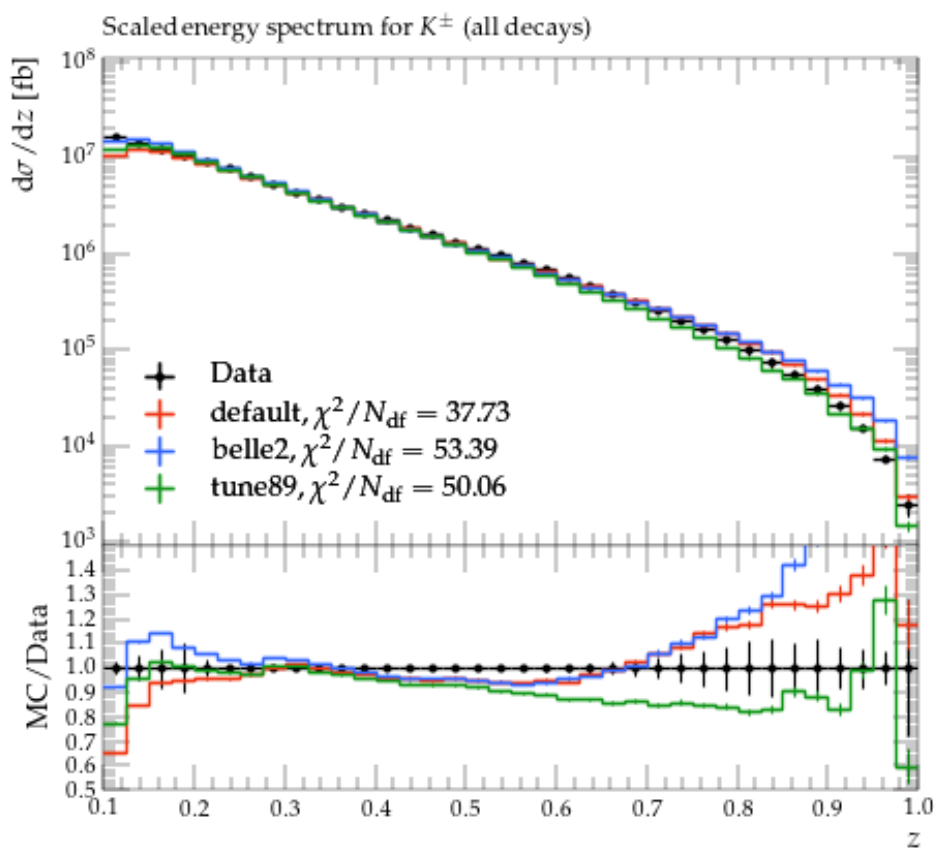


Figure 54: Kaon cross sections as a function of the fractional energy z . The data is displayed by black points while the PYTHIA default is displayed in red, the current Belle2 setting in blue, and the best tune in green.

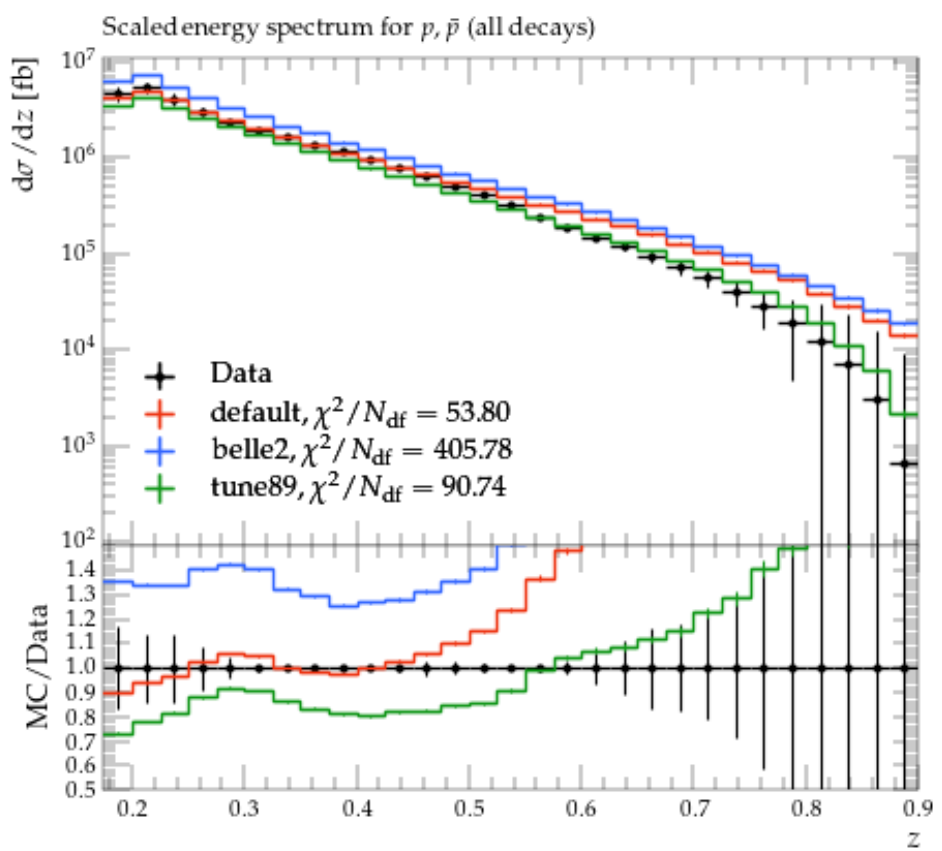


Figure 55: Proton cross sections as a function of the fractional energy z . The data is displayed by black points while the PYTHIA default is displayed in red, the current Belle2 setting in blue, and the best tune in green.

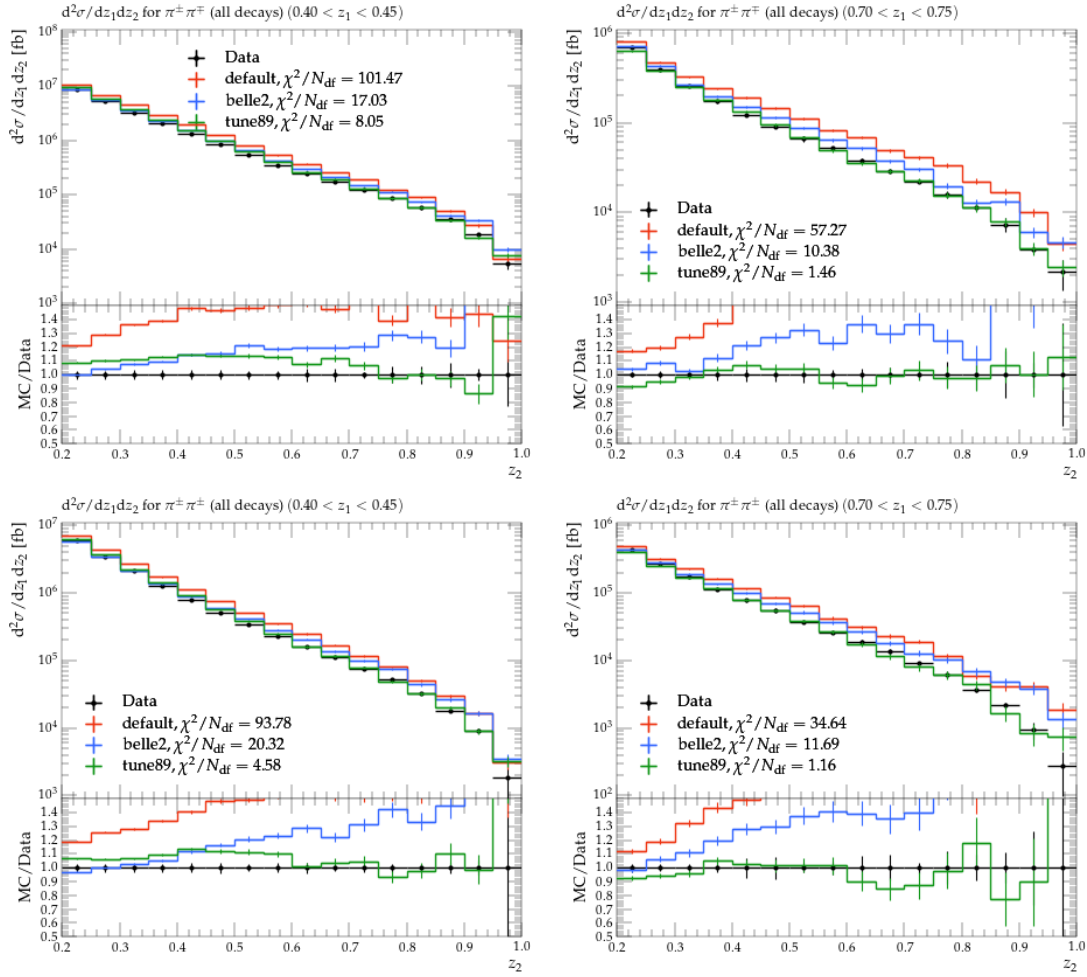


Figure 56: Top: $\pi^+\pi^-$ spectra as a function of z_2 for two bins of z_1 . Bottom: $\pi^\pm\pi^\pm$ spectra for the same z bins. The data is displayed by black points while the PYTHIA default is displayed in red, the current Belle2 setting in blue, and the best tune in green.

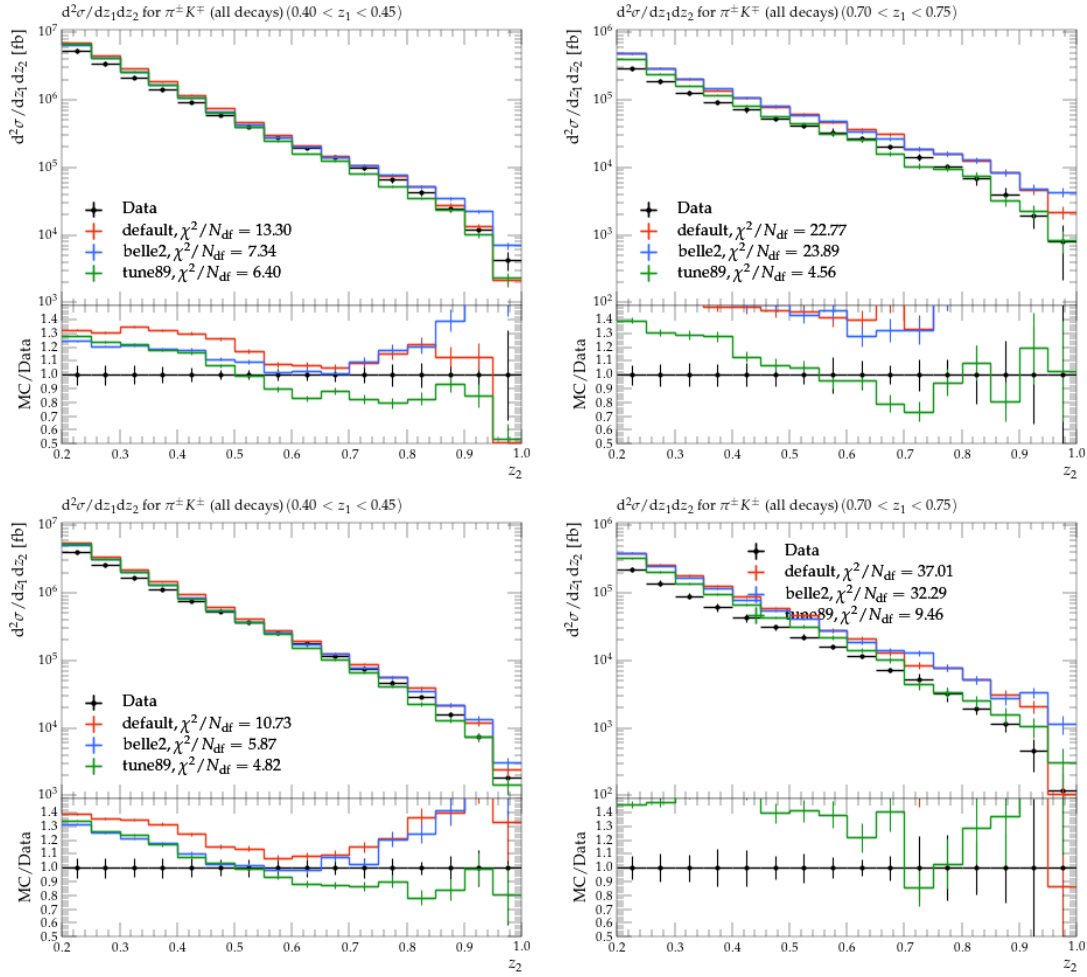


Figure 57: Top: π^+K^- spectra as a function of z_2 for two bins of z_1 . Bottom: $\pi^\pm K^\pm$ spectra for the same z bins. The data is displayed by black points while the PYTHIA default is displayed in red, the current Belle2 setting in blue, and the best tune in green.

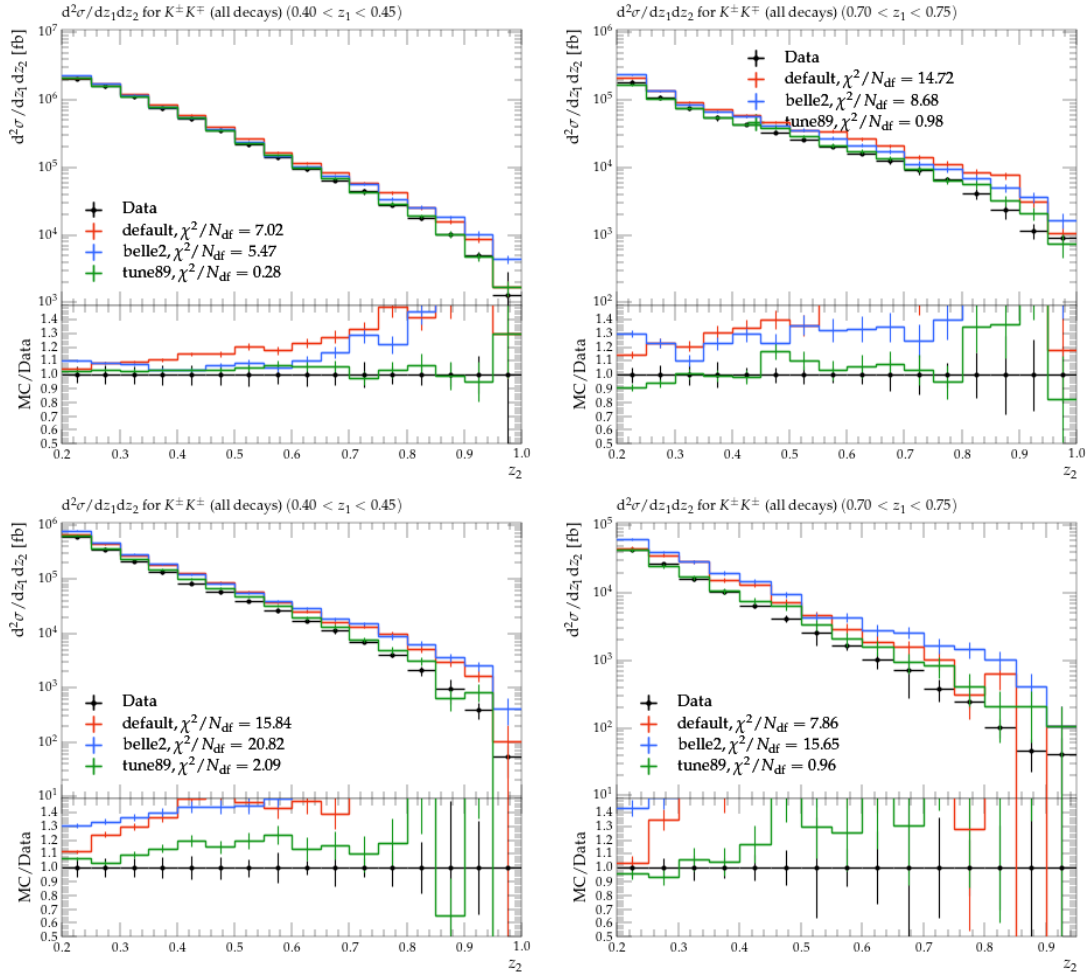


Figure 58: Top: K^+K^- spectra as a function of z_2 for two bins of z_1 . Bottom: $K^\pm K^\pm$ spectra for the same z bins. The data is displayed by black points while the PYTHIA default is displayed in red, the current Belle2 setting in blue, and the best tune in green.

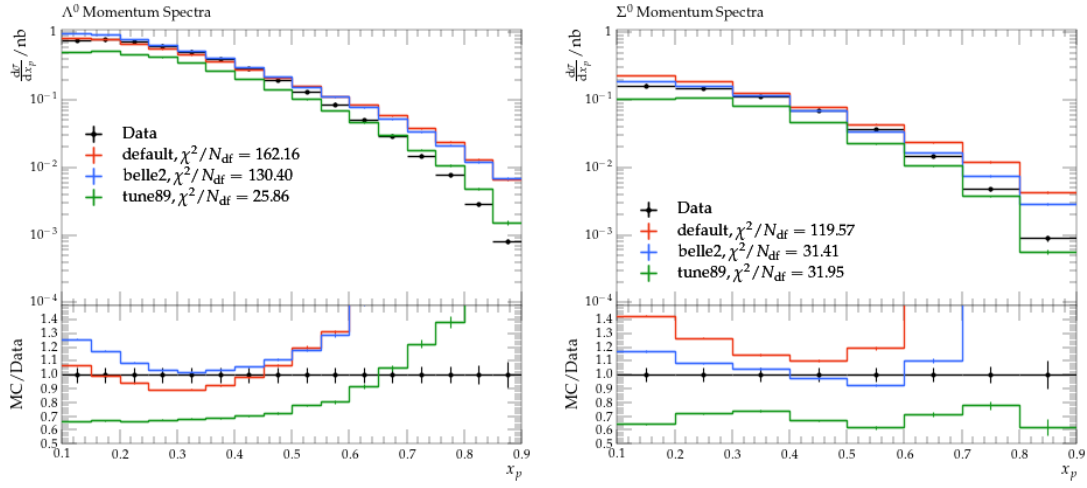


Figure 59: Left: Λ spectrum as a function of x_p . Right Σ^0 spectrum as a function of x_p . The data is displayed by black points while the PYTHIA default is displayed in red, the current Belle2 setting in blue, and the best tune in green.

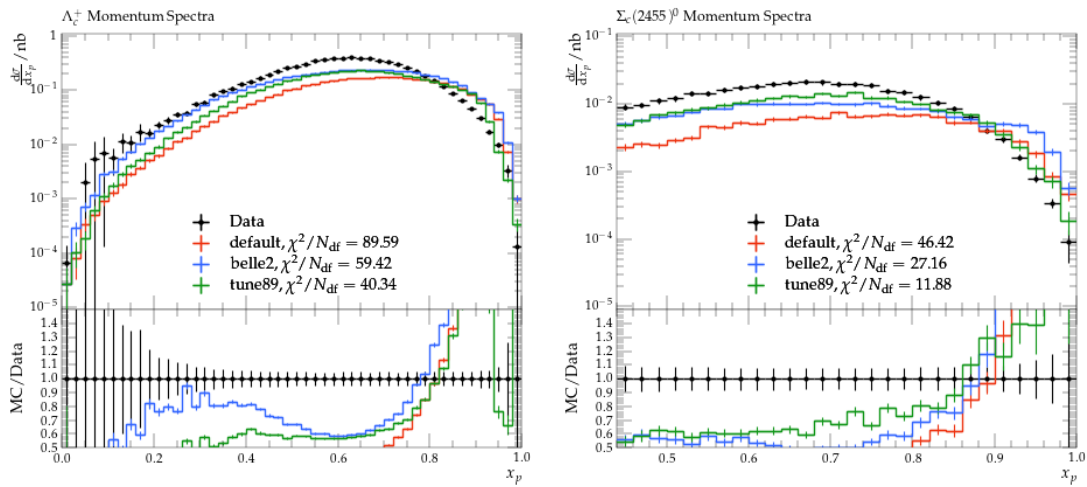


Figure 60: Left: Λ_c^+ spectrum as a function of x_p . Right $\Sigma_c(2455)^0$ spectrum as a function of x_p . The data is displayed by black points while the PYTHIA default is displayed in red, the current Belle2 setting in blue, and the best tune in green.

Table 2: Best tune variables and the variation of the best values during the various tune iterations.

Variable	Best results	default
StringZ:ALund	0.592 -0.067 +0.253	0.680
StringZ:BLund	1.080 -0.170 +0.036	0.980
StringFragmentation:StopM	0.734 -0.050 +0.535	0.800
StringFlav:etaSup	0.649 -0.301 +0.221	0.600
StringFlav:StoUD	0.240 -0.006 +0.004	0.217
StringFlav:SigmaKt	0.372 -0.019 +0.000	0.335
StringFlav:mesonUDvector	0.565 -0.109 +0.138	0.500
StringFlav:mesonUDL1S0J1	0.556 -0.306 +0.108	0
StringFlav:mesonUDL1S1J0	0.411 -0.234 +0.000	0
StringFlav:mesonUDL1S1J1	0.226 -0.000 +0.086	0
StringFlav:mesonUDL1S1J2	0.341 -0.061 +0.399	0
StringFlav:mesonSvector	0.836 -0.163 +0.498	0.550
StringFlav:mesonSL1S0J1	0.229 -0.110 +0.459	0
StringFlav:mesonSL1S1J0	0.469 -0.094 +0.243	0
StringFlav:mesonSL1S1J1	0.872 -0.489 +0.000	0
StringFlav:mesonSL1S1J2	0.370 -0.207 +0.001	0
StringFlav:mesonCvector	1.740 -0.882 +0.486	0.880
StringFlav:mesonCL1S0J1	0.865 -0.634 +0.864	0
StringFlav:mesonCL1S1J0	0.300 -0.252 +0.408	0
StringFlav:mesonCL1S1J1	0.772 -0.129 +0.145	0
StringFlav:mesonCL1S1J2	0.170 -0.084 +0.198	0
StringZ:rFactC	1.069 -0.658 +0.383	1.32
StringFlav:probQQtoQ	0.064 -0.002 +0.008	0.081
StringFlav:probSQtoQQ	0.497 -0.398 +0.184	0.915
StringFlav:probQQ1toQQ0	0.065 -0.000 +0.864	0.0275
StringZ:aExtraDiquark	1.487 -0.785 +0.420	0.970
StringFlav:popcornRate	0.734 -0.000 +0.104	0.500
StringFlav:popcornSpair	0.350 -0.016 +0.000	0.500
StringFlav:popcornSmeson	0.180 -0.000 +0.139	0.900
StringFlav:thetaPS	57.719 -78.753 +10.675	-15.
StringFlav:thetaV	24.353 -0.952 +24.444	26.

554 9 Results

555 The best results of the tuning exercise are already tabulated in table 1 together with
556 the default values used in PYTHIA8.3 and BelleII. The overall confidence in the best
557 results is high as indicated by the data-tune comparisons in the previous chapters.
558 There are however different levels of how confident the best variables are depending
559 on the overall sensitivities. Based on those, the main Lund parameters are probably
560 very well determined by the tuning as the sensitivities are very high. The vector me-
561 son related variables are also fairly well determined thanks to the latest Belle paper
562 [3] which explicitly looked at the fragmentation of vector mesons. The higher spin
563 related variables are somewhat less determined due to the fact that no explicit mea-
564 surements of these particles are available. There is some indirect sensitivity via the
565 invariant mass distributions where the higher mass ranges get populated from such
566 particle decays. Last, the baryon related variables seem to be also well-determined,
567 but it is obvious by the differences from the tune to the data that the description of
568 baryon fragmentation in the Lund model seems to be still lacking. It will be still bet-
569 ter to use the optimized values, but there need to be also significant improvements
570 on the model description itself to really obtain a very reliable description of bary-
571 onic final states. As a next step for the BelleII continuum simulation development,
572 it will be important to see whether the optimized settings also directly translate into
573 significant improvements within the overall BelleII simulation framework that uses
574 EvtGen for decays rather than the standalone PYTHIA used in these studies.

575 References

576 [1] Bo Andersson, G. Gustafson, G. Ingelman, and T. Sjostrand. Parton Frag-
577 mentation and String Dynamics. *Phys. Rept.*, 97:31–145, 1983. doi:10.1016/
578 0370-1573(83)90080-7.

579 [2] Bo Andersson. *The Lund Model*, volume 7. Cambridge University Press, 1998.
580 doi:10.1017/9781009401296.

581 [3] R. Seidl et al. Production cross sections of light and charmed mesons in e+e-
582 annihilation near 10.58 GeV. *Phys. Rev. D*, 111(5):052003, 2025. arXiv:2411.
583 12216, doi:10.1103/PhysRevD.111.052003.

584 [4] Andy Buckley, Hendrik Hoeth, Heiko Lacker, Holger Schulz, and Jan Eike von
585 Seggern. Systematic event generator tuning for the LHC. *Eur. Phys. J. C*,
586 65:331–357, 2010. arXiv:0907.2973, doi:10.1140/epjc/s10052-009-1196-7.

587 [5] M. Niiyama et al. Production cross sections of hyperons and charmed baryons
588 from e^+e^- annihilation near $\sqrt{s} = 10.52$ GeV. *Phys. Rev. D*, 97(7):072005, 2018.
589 arXiv:1706.06791, doi:10.1103/PhysRevD.97.072005.

590 [6] R. Seidl et al. Invariant-mass and fractional-energy dependence of inclusive
591 production of di-hadrons in e^+e^- annihilation at $\sqrt{s} = 10.58$ GeV. *Phys. Rev. D*,
592 96(3):032005, 2017. arXiv:1706.08348, doi:10.1103/PhysRevD.96.032005.

593 [7] R. Seidl et al. Transverse momentum dependent production cross sections of
594 charged pions, kaons and protons produced in inclusive e^+e^- annihilation at
595 $\sqrt{s} = 10.58$ GeV. *Phys. Rev. D*, 99(11):112006, 2019. arXiv:1902.01552, doi:
596 10.1103/PhysRevD.99.112006.

597 [8] R. Seidl et al. Update of inclusive cross sections of single and pairs of identified
598 light charged hadrons. *Phys. Rev. D*, 101(9):092004, 2020. arXiv:2001.10194,
599 doi:10.1103/PhysRevD.101.092004.

600 A Pythia StringZ:aExtraDiquark bugfix related 601 changes

602 As indicated in communication by the PYTHIA team, a bug was found in their port-
603 ing of the String fragmentation routines from fortran-based sc pythia6 to PYTHIA8
604 which persisted until version 8.3.14. This bug was related to the handling of the
605 variable StringZ:aExtraDiquark. This behavior was fixed in later versions, but since
606 most tuning efforts using older versions obtained best parameters that included this
607 bug, a switch was introduced to still use the old, incorrect treatment or the corrected
608 one by: StringZ:useOldAExtra = on/off. To test the actual behavior on the Belle2
609 tuning efforts, the best tune iteration at that time (tune71) was compared for the
610 old, previously used PYTHIA version 8.3.13, and the latest version 8.3.16 either hav-
611 ing the old or new treatment explicitly switched on or off. As expected, these changes
612 had no visible effect on any of the meson related measurements used in the tune op-
613 timization. When using the old treatment, also no sizable changes were observed for
614 the various baryon measurements, but the behavior between old and new treatment
615 was significantly different. As intended for this variable, the high- z or x_p shapes be-
616 came softer with the new treatment which resulted in a generally better description
617 of the proton cross sections. Also the behavior of hyperon and charmed baryon cross
618 sections visibly improved while the overall magnitudes are still not well described.
619 The corresponding comparisons are shown in Figs. 61 and 62 for protons, several
620 hyperons and charmed baryons. In these comparisons, it is also visible that the de-
621 fault behavior (i.e. without explicitly setting the StringZ:useOldAExtra = on/off
622 variable) corresponds to the old setting. Because of these changes, and the improve-
623 ments that go with them, the remainder of the tuning effort was performed using
624 the PYTHIA version 8.3.16 and using the new treatment via StringZ:useOldAExtra
625 = off.

626 Initially, it was not clear, that the old treatment is still used per default, which re-
627 sulted in the first tuning efforts after this switch to still use it. Only from tune76 for-
628 ward the new, correct treatment was explicitly implemented via StringZ:useOldAExtra
629 = off.

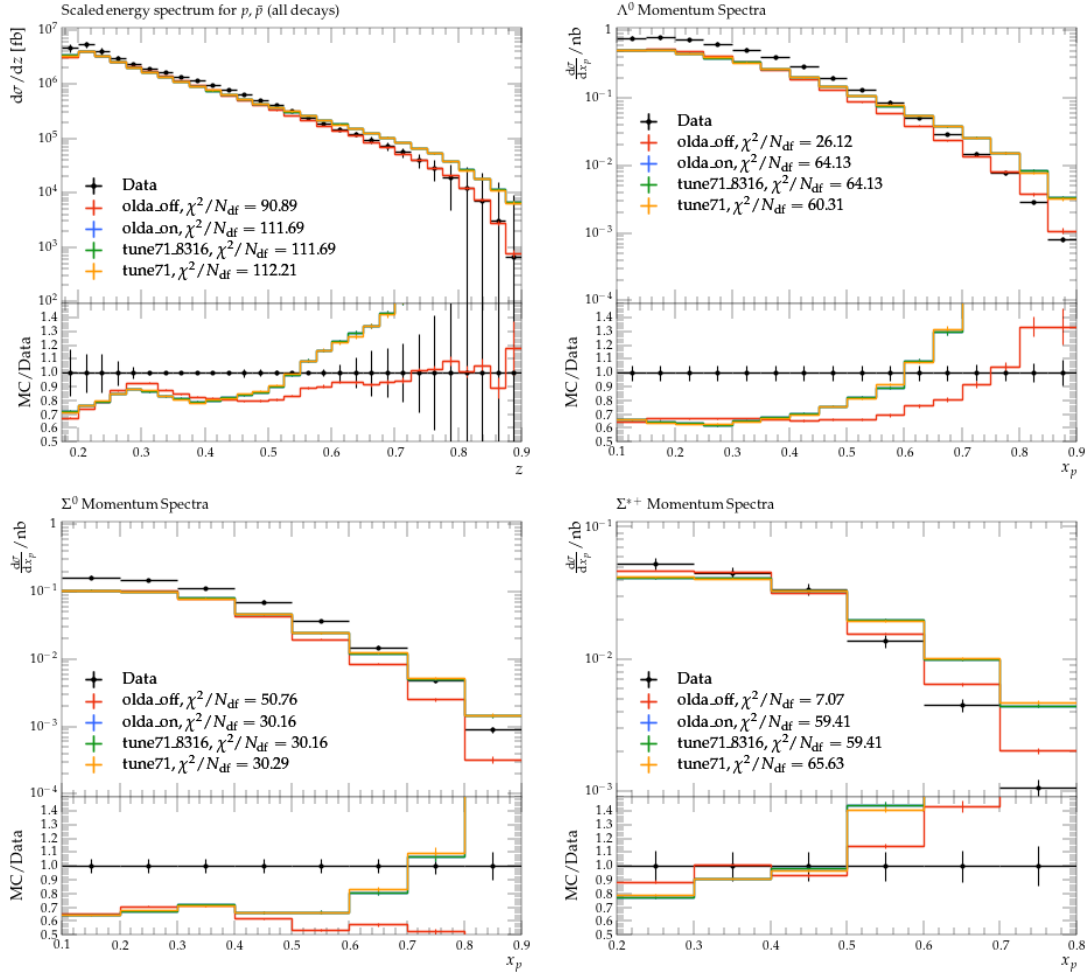


Figure 61: Comparison of the distributions for protons (top left), Λ (top right), Σ^0 (bottom left) and Σ^{*+} as a function of energy or momentum fraction. The black points correspond to the measurements while the yellow points correspond to the best values after tune 71 using PYTHIA8.3.13, the green points correspond to the same tune but using PYTHIA8.3.16, the blue points use the same but explicitly setting `StringZ:useOldAExtra` to "on", and the red points correspond to the same, but switching it to "off".

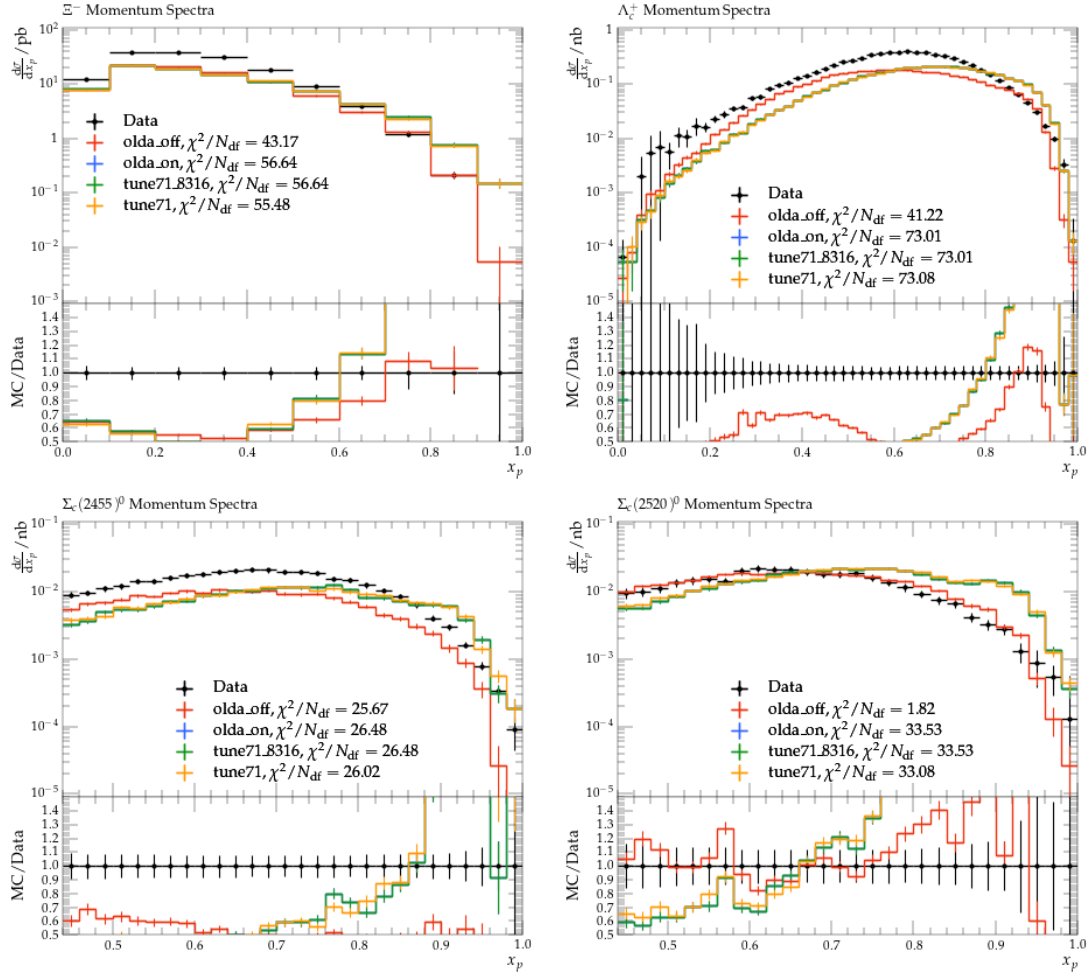


Figure 62: Comparison of the distributions for Ξ^- (top left), Λ_c (top right), $\Sigma_c^0(2455)$ (bottom left) and $\Sigma_c^0(2520)$ (bottom right) as a function of momentum fraction. The black points correspond to the measurements while the yellow points correspond to the best values after tune 71 using PYTHIA8.3.13, the green points correspond to the same tune but using PYTHIA8.3.16, the blue points use the same but explicitly setting `StringZ:useOldAExtra` to "on", and the red points correspond to the same, but switching it to "off".